Biomimetic sea-cucumber: stiffness fast-reversible, turbidity switchable, shape-memorable and self-healing hydrogel

By

Ruijia Yang

A Thesis Submitted to the Faculty of Graduate Studies of

The University of Manitoba

In partial fulfillment of the requirements of the degree of

Master of Science

Department of Mechanical Engineering

University of Manitoba

Winnipeg, Manitoba

Abstract

Natural biological models that possess attractive features clue us on the designing of smart devices. Echinoderms such as sea cucumbers lead the way to design stimuli-responsive stiffness-change materials; self-recovery abilities of skin inspire the generation of self-healing materials; and the touch-sensitive behaviors of mimosas spark the concept of shape-memory. Hydrogels are wildly used as biomaterials, and those with multifunctionalities have attracted widespread attention due to their potential in the biomedical area. However, the successful construction of multifunctional hydrogels remains a challenge because the desired functions are always hard to be tailored together. Therefore, the means to successfully build these hydrogels are of great demand. This study reports a stimuli-responsive hydrogel based on the double network (DN) system, and it shows biomimetic functions such as tremendous reversible stiffness changes, outstanding shape-memory and self-healing abilities. The hydrogel consists of carboxymethyl-chitosan (CM) and acrylamide (AM) where the AM network is set to be the primary network to provide a soft matrix, while the CM network is set to be the second network that can be reversibly generated/eliminated through cyclic acid-base treatments. Due to this mechanism and the inherent rigid property of the CM network, this hydrogel exhibits reversible stiffness changes (an increase by a factor of 100 of compressive modulus), excellent self-healing capabilities (91% of self-healing efficiency) and outstanding shape-memory performances (~100% of shape-fixing efficiency and ~97% of shape-recovery ratio). The DN hydrogel can be applied as motion sensors, “on-demand” switches and “LEGO-like” 3D printing ink. In summary, this study presents a new strategy to fabricate multifunctional hydrogels that can have great potential in the biomedical area.

Acknowledgments

First of all, I'd like to give my sincere thankfulness to my advisor Dr. Malcolm Xing for giving me the opportunity to study with him and supporting me with high professionalism, knowledgeable guidance and patient instruction throughout these years.

Besides, I would like to thank my thesis committee members, Dr. Chuang Deng and Dr. Wen Zhong for their valuable comments and professional assistance.

Furthermore, I owe deeply gratefulness to my family, specifically my mother and father, for their endless love, selfless support and always respecting my decisions. They open up a broader world for me and help me realize what I want in my life.

I also want to thank all members of the Mechanical Engineering Lab for their research assistance and being good companions of mine.

Table of Contents

Abstract I

Acknowledgments II

List of Figures VI

List of Schemes X

List of Copyrighted Materials for which Permission was Obtained XI

List of Abbreviations XII

Chapter 1 Introduction 1

1.1 General Overview 1

1.2 Problem Definition 4

1.3 Objective 6

1.4 Summary of Experimental Methods and Major Findings 7

1.4.1 Summary of Experimental Methods 7

1.4.2 Summary of Major Findings 7

1.5 Thesis Layout 9

Chapter 2 Literature Review 10

2.1 Hydrogels 10

2.1.1 Nanocomposite Hydrogel Systems 13

2.1.2 Hybrid Hydrogel Systems 17

2.1.3 Double Network hydrogel systems 19

2.2 Bioinspired Stimuli-Responsive Hydrogel Systems 23

2.2.2 Self-Healing Hydrogels 29

2.2.3 Shape-Memory Hydrogels 32

2.2.4 Multifunctional Hydrogels 35

2.3 Recent Advancement on CM-Based Hydrogels 36

2.3.1 Polysaccharide-based Hydrogels 36

2.3.2 Current Advancement on Chitosan-based and CM-Based Hydrogels 36

Chapter 3 Experimental Proceders 39

3.1 Introduction 39

3.2 Materials 39

3.3 Preparation and Characterization of CM-Based DN Hydrogels 40

3.3.1 Preparation of CM Hydrogels 40

3.3.2 Preparation of AM Hydrogels 40

3.3.3 Preparation of Pristine Hydrogels 40

3.3.4 Preparation of CM-Based DN Hydrogels 41

3.3.5 ^{1}H NMR Spectra 41

3.3.6 FT-IR Characterization 42

3.3.7 Scanning Electron Microscopy (SEM) Imaging 42

3.3.8 Swelling Ratio Tests 42

3.3.9 Rheology Characterization 43

3.4 Multifunctionality Tests 43

3.4.1 Sample Preparations 44

3.4.2 Macroscopic Tests 45

3.4.2 Tensile and Compressive Tests 46

3.4.3 Statistic Analysis 46

3.5 Potential Applications 46

3.5.1 Sample Preparations 46

3.5.2 Motion-Sensing and "on-demand" switch 47

3.5.3 LEGO-Like 3D Printing Ink 48

Chapter 4 Results and Discussion 49

4.1 Introduction 49

4.2 Preparation and Characterization of CM-Based DN Hydrogels 49

4.2.1 Preparation of CM-Based DN Hydrogels 49

4.2.2 Characterization of CM-Based Hydrogels 52

4.3 Multifunctionality Tests 63

4.3.1 Reversible Stiffness Changes Behavior 63

4.3.2 Self-Healing Performance 72

4.3.3 Shape-memory Ability 77

4.4 Potential Applications 81

4.4.1 Motion Sensor and "On-demand" Switch 81

4.4.2 "LEGO-Like" 3D Printing Ink 83

Chapter 5 Summary and Conclusions 85

Chapter 6 Suggestions for Future Work 87

References 88

Appendix 97

List of Figures

Figure 1 Hydrogel classifications fall into seven categories[51]. 12

Figure 2 A general view of the applications of nanocomposite hydrogels[52]..... 14

Figure 3 A general summary about material properties[84]. 22

Figure 4 (a) Representation of the interactions between CNC−COOH and CNC−NH_2 at different pH; (b) Synthesis process[95]..... 28

Figure 5 Schematic representation of the synthesis of the mono-N-carboxymethyl chitosan (MCC)[140]. 38

Figure 6 Photographic images of a) CM hydrogel, b) AM hydrogel, c) Pristine hydrogel, d) DN hydrogel and e) DN hydrogel treated with base for 1min. f) Tensile curves of pristine and AM hydrogels, insert is the photo of tensile tests. 51

Figure 7 ^{1}H NMR spectra of CM molecules. 53

Figure 8 FT-IR images of (top) CM and (bottom) CM gel. 57

Figure 9 Swelling ratio results. a) Column graph of swelling ratio of different hydrogels at swelling equilibrium stage (n=3). b) Swelling ratio of different hydrogels after predetermined time points(n=3). Photographic images of volume changes of (from left to right) CM, AM, pristine and DN gels after being incubated in DI water for c) 0h, d) 4h, e) 12h, f) 48h, g) 72h and h) 120h. 58

Figure 10 SEM images of a) CM gels, b) AM gels, c) pristine gels, d) DN gels and e) DN gels after basic treatments for 15min. Scale bars = 30μm. 60

Figure 11 Frequency sweep results of CM, AM, pristine and DN hydrogels showed the good stability of the DN hydrogel during the angular changes of 0.1-100 rad s^{-1} (1% strain). 62

Figure 12 a) Pristine hydrogel strip was soft. b) Hydrogel at the P stage after acidic treatments (0.1M HCl) for 1min became stiff enough to withstand its own weight. c) After basic treatments (0.3M NaOH) for another 1min, hydrogel trip transited to the D stage and regained its softness. d) Compressive curves of DN and pristine hydrogels. e) The maximum compressive stress of DN and pristine hydrogels. f) Compressive modulus of DN and pristine hydrogels. g) Tensile curves of DN and pristine hydrogels. h)The maximum stress of DN and pristine hydrogels. i) Tensile elastic modulus of DN and pristine hydrogels. (n=3) 64

Figure 13 SEM images of a) pristine hydrogels, b) DN-1-5% hydrogels, c) DN-5-5% hydrogels, d) DN-15-5% hydrogels, e) DN-30-1% hydrogels, f) DN-30-3% hydrogels and g) DN-30-5% hydrogels. Scale bars = 30μm. 67

Figure 14 a) Compressive curves of DN-x-5% hydrogels, where x=1, 5, 15, 30. b) Compressive modulus of DN-x-5% hydrogels, where x=1, 5, 15, 30. c) Compressive curves of DN-30-y hydrogels, where y=1, 3, 5. d) Compressive modulus of DN-30-y hydrogels, where y=1, 3, 5. e) Compressive curves of DN-x-5% hydrogels, where x=1, 5, 15, and the acid used here to induce CM network was 0.3M HCl. f) Compressive modulus changed as acidic incubation time increased, and a higher acidic concentration accelerated the speed to achieve the

maximum stiffness change. g) Compressive strain at break for different hydrogels. (n=3) . 68

Figure 15 Optical changes of DN hydrogels under the treatments of different acidic solutions at predetermined time points. 69

Figure 16 a-c) Compressive curves of the first/second/third acid-base cyclic tests. d) Compressive stress of hydrogels at diverse stages (n=3). e) G' and G'' as a function of hydrogels at different stages. Each treatment lasted for 1min. 71

Figure 17 Macroscopic self-healing tests: a) before acid the hydrogel strip had a wedge and "heart" was broke into halves, b) after acidic treatment, both of them healed, c) then they were placed in DI water for 3h and remained integration showing that the healing was caused by physical interactions (CM network) rather than simple adhesion, d) while after basic treatment, the wedge reappeared and the "heart" again separated into halves. e) The results of G' and G'' of the pristine hydrogels at strain amplitude sweep tests ranging from 1% to 700% at a fixed angular frequency at 10 rad s^{-1}. f) The sol-gel transformation of CM gel in the presence of external stimuli proved that the self-healing was a result of the formation/elimination of the CM network. 73

Figure 18 Tensile strengths of a) DN-x-1%, b) DN-x-3% and c) DN-x-5% hydrogels, where x = 15, 30 and 60. (n=3) 75

Figure 19 a) Self-healing tests were conducted on this end-to-end model. b) Self-healing efficiency of DN hydrogels under different acidic solutions (0.1/0.3M HCL). c-d) The SE of DN hydrogels increased under prolonged acidic treatments. e-f) The SE of DN hydrogels with

different initial CM concentrations, in here, the SE was compared between the tensile stress of healed ones (dotted lines) and the tensile stress of the un-cut ones (solid lines) with the same CM concentrations, i.e., the healed SE-1% compared to the uncut DN-1%. (n-3) 76

Figure 20 Fast shape-memory behaviors of the CM-based DN hydrogel. a-c) Twisted model. d-f) Elongation model.)g-i Expanded model. 79

Figure 21 a) Shape-fixing efficiency profile of hydrogels at $P_{1/2/3}$ stages, black hollow squares represent fixity measurement conducted to hydrogels placed in DI water while red hollow circles represent fixity results of hydrogels placed in hermetical containers. b) Length, width, thickness and weight changes for P_1 hydrogels after being placed in hermetical containers for 3 hours. c) Hydrogel strip samples' lengths at different stages. d) Shape-recovery ratio of hydrogels at $D_{1/2/3}$ status. (n=3) 80

Figure 22 a) The resistances of pristine, DN-1-5%, DN-2-5% and DN-3-5% hydrogels. b) Illustration of the motion sensor device. Hydrogel works as a motion sensor, the relative resistance defined as $(R-R_0)/R_0$ as a function of time were introduced to measure the sensitivity, results of c) 45˚ bend and d) 90˚ bend. e-f) One flat hydrogel strip was fixed into a temporary shape with a curvature of 90˚using 0.1M HCl, it was then attached to one cupper strip in a circuit where another cupper strip was distantly placed beside. 82

Figure 23 a-d) Illustration of three-step 3D printing. Examples of "LEGO" property, e,f)Olympic rings, g-h) Christmas trees, i-j) airplanes. 84

Figure 24 Product information sheet of CM. 97

List of Schemes

Scheme 1 Schematic illustration of the mechanism of CM-based DN hydrogel. 55

List of Copyrighted Materials for which Permissions were Obtained

Figure 1: Source - Journal Materials Science and Engineering. Reprinted from Ullah et al., Journal of Materials Science and Engineering, 2015. 57: p. 414-433. With permission from Elsevier.

Figure 2: Source – Colloid and Polymer Science. Reprinted from Schexnailder, P., G.J.C. Schmidt, and P. Science, Colloid and Polymer Science, 2009. 287(1): p. 1-11. With permission from Springer Nature.

Figure 3: Source - Journal of Materials Chemistry B. Reprinted from Li, J., Z. Suo, and J.J.J.J.o.M.C.B. Vlassak, Journal of Materials Chemistry B., 2014. 2(39): p. 6708-6713. With permission from Royal Society of Chemistry.

Figure 4: Source - ACS Macro Letters. Reprinted from Way et al., ACS Macro Letters, 2012. 1: p. 1001-1006. With permission from American Chemical Society.

Figure 5: Source - Journal of pharmaceutical sciences. Reprinted from M et al., Journal of pharmaceutical sciences 2001. 90(1): p. 38-46. With permission from Elsevier.

List of Abbreviations

AM	Acrylamide
APS	Ammounium Persulfate
CNTs	Carbon Nanotubes
CM	Multi-walled Carboxymethyl Chitosan
D_n	Deprotonated Stage
DI	Deionized
DN	Double Network
ECM	Extracellular Matrix
F	Shape-fixing Efficiency
FT-IR	Fourier Transformed Infrared
G’	Storage Modulus
G’’	Loss Modulus[1]H
HAp	Hydroxyapatite
LED	Light Emitting Diode

MBA	N, N'-Methylenebis(acrylamide)
NMR	Proton Magnetic Resonance
P_n	Protonated Stage
PAM	Poly (acrylamide)
PEG	Polyethylene Glycol
RR	Shape-recovery Ratio
SEM	Scanning Electron Microscope
SR	Self-healing Ratio
TEMED	N, N, N, N'-Tetramethylethylnendiamine (TEMED)
UV	Ultraviolet Radiation

Chapter 1

Introduction

1.1 General Overview

Hydrogels consist of 3D polymer networks that contain a large amount of water, and they are wildly studied to have numerous applications in areas like biomedical devices[1] , tissue engineering[2, 3], soft robots[4, 5], wearable electronics[6, 7], etc. Bio-inspired design is an approach to generate, improve, and integrate fascinating properties seen in nature by applying biological principles[8]. Natural models are capable of performing physiochemical changing abilities such as reversible stiffness, shape-memory and self-healing. And they provide countless ideas for the designing of hydrogels with intriguing features. For instance, reversible stiffness change is commonly seen in many echinoderms, such as sea cucumber, sea urchin, etc. This morphing is considered to be the defense mechanism that provides them with vital survival skill. The stiffness of materials has a great influence on their biological uses, for example, recent researches have shown that ECM's stiffness has a significant influence on cell contractility, migration, spreading and differentiation[9, 10].

Shape memory is found in animals and plants such as octopuses' movements and the press-sensitive closing of mimosas. Shape-memory materials are normally defined as those that can't go back to their original shapes once a deformation is made unless external stimuli (pH, light, thermos, etc.) apply[11]. They have ample applications such as controlled drug delivery and release[12, 13],

bio-actuators, etc[14]. Self-healing is also very commonly found in animals such as lizards, earthworms, etc. Materials with self-healing abilities have been demonstrated as ones that can repair themselves following damages automatically or upon exposing to external triggers, during which the typical interactions are based on dynamically reversible covalent and/or non-covalent interactions[15, 16]. This property offers materials substantial benefits such as maintaining structural integrity and elongated use term[17, 18]. Therefore, hydrogels with multi-functionalities as mentioned above are expected to have a great potential to broaden hydrogel's applications in the biomedical area.

Researches have demonstrated a mechanism called "stimuli-responsive mechanical adaptivity" that can cause significant stiffness changes by utilizing the switchable hydrogen bonds between cellulose nanofibers[19]. The same switchable mechanically adaptive principle can also be used to endow materials with shape-memory abilities by combining an elastic matrix (providing deformation ability) and a switchable element (performing shape programming, fixing and recovery by stimulators)[20]. Another mechanism used to perform stiffness changes is to obtain metastability in materials. Yang et al. reported a hybrid hydrogel system that can perform reversible stiffness changes between two stable solid states by physical metastability, the underlying mechanism was to use the transformation of a supercooled liquid that had an energy barrier between its two states[21]. However, their method is limited in materials with physical metastability (supercooling) which hindered its versatility.

In the case of self-healing, the fusion of the wounded sites are commonly achieved by dynamic covalently/non-covalently cross-linked chains[22-24]. A more biomimetic approach in a similar

fashion to blood clotting based upon biological “bleeding” mechanism was reported where the healing monomers were released into the cracked sites, coming into contact with each other and catalyzed by a dispersed catalyzer[25, 26].

Recently, polysaccharide-based hydrogels have attracted increasing attention because of their biodegradability, biocompatibility, and bioactivity[27]. Agarose, chitosan, alginate, hyaluronic acid and cellulose are commonly seen polysaccharide classes, among them, chitosan is of great importance because it is the only naturally cationic polysaccharide. Chitosan is the fully or partially de-acetylated derivative of chitin, and its potential has been proved in the biomaterial field[2, 28, 29]. Studies have shown that partially de-acetylated chitosan can form “onion-like” hydrogels through physical interactions such as hydrophobic interactions, hydrogen bonds and crystallite formation via repeated neutralization of $-NH_3^+$ sites under basic treatments[30]. Carboxymethyl-chitosan (CM) is the water-soluble derivative of chitosan, and the CM-based hydrogels are mostly used as pH-sensitive drug delivery vehicles. Moreover, carboxymethyl cellulose-based hydrogel is reported to have reversible stiffness, shape-memory and self-healing functions[31]. AM gels are highly ductile and stable and have been broadly used as the matrix in the construction of DN hydrogels.

1.2 Problem Definition

Multifunctional hydrogels have broad applicability due to their enhanced mechanical property, better adaptability, greater integration of features, etc. Hydrogels engaging such properties are desirable materials yet uncommon and challenging. One of the limitations of current methods to produce these multifunctional hydrogels is that the features cannot always be tailored together. For example, self-healing hydrogels often suffer poor mechanical strength, it is because self-healing ability comes out of dynamic bonds that can be easily broken and reformed, while the "unstable" cross-links are one of the reasons causing mechanical weakness during the experimental time[23]. To date, only a few researches have been reported on hydrogels with reversible stiffness along with shape-memory and self-healing abilities. And the ways to produce them are always complicated in either molecular designs (i.e., DNA-based carboxymethyl-cellulose hydrogel) or regulation conditions (i.e., thermally or UV based)[31-34]. Therefore, more convenient ways to fabricate multifunctional hydrogels are of high demand and in continuous exploration.

Sole hydrogels are limited in applications due to their poor mechanical performances. Therefore, countless efforts have been devoted to improving the mechanical properties including double-network gels[35], nanocomposite gels[36], hybrid gels, etc[37, 38]. Conventionally, DN hydrogels are composed of two steps of polymerizations during which one covalent cross-linking network is induced to play the primary role and one non-covalent cross-linking network is set to play the sacrificial role[39, 40]. DN hydrogels are well studied due to their high rigidity and toughness, superior compressive and tensile properties[39-41]. Despite the extensive studies, only a few attempts were made to demonstrate the multi-functionality of this kind.

In addition, most studies aim to study the drug delivery behaviors of CM-based hydrogels, and the gelation of CM is normally obtained ionically (Ca^{2+}), chemically (glutaraldehyde) or by blending with other ionic complexes (alginate). Acid-induced gelation has never been employed let alone the utilization of its underlying mechanism into the fabrication of multifunctional hydrogels.

1.3 Objective

The overall objective of this project was to design a hydrogel based on CM molecules to achieve the construction of the multifunctional hydrogel. In details, it aimed to realize acid-base-induced reversible stiffness transitions along with outstanding shape-memory and self-healing properties. The as-designed system could open up a new door for the fabrication of multifunctional hydrogels with great potential in biomedical areas. To achieve these objectives, the following works were established:

1. Confirmation of the formation of the CM network through various characterization methods.
2. Incorporating the CM network into the PAM network to obtain pristine hydrogels.
3. Conducting microscopic, macroscopic and mechanical tests to prove the multi-functionality of the CM-based DN hydrogels.
4. Conceptual application demonstrations to show the potential of this hydrogel system.

1.4 Summary of Experimental Methods and Major Findings

1.4.1 Summary of Experimental Methods

The chemical structure of CM was confirmed by Proton Magnetic Resonance (^{1}H NMR) (Bruker Avance 300MHz NMR spectrometer), the underlying mechanism of property changes was analyzed by macroscopic, Fourier transform infrared (FT-IR) spectra (Thermo Nicolet iS FTIR spectra), scanning electron microscope (SEM) (Quanta FEG 650), rheology (TA Discovery Hybrid Rheometer) and swelling ratio tests. The stiffness change, self-healing and shape-memory abilities were vividly exhibited by macroscopic experiments, then quantitatively measured by mechanical tests (INSTRON 5965) which included compressive and tensile tests. In details, Young's modulus, self-healing efficiency, shape-fixing and shape-recovery ratio were used for measurements. In addition, influence factors such as the concentrations of initial CM and conditions of the external stimulus were also discussed. In the end, three conceptual applications were tested.

1.4.2 Summary of Major Findings

Macroscopic tests showed the reversible acid-base-induced formation/elimination of the CM network. The AM gels incorporated with CM molecules (pristine hydrogels) exhibited great ductility. After acidic treatments, the obtained DN hydrogels had significantly higher stiffness while they regained their softness after basic treatments. The self-healing and shape-memory properties were also observed by macroscopic tests.

FT-IR, SEM and rheology tests had shown that the formative mechanism should be ascribed to the

generation and elimination of the physical CM network through protonation and deprotonation of $–COO^-$ groups of CM molecules, and the CM network was formed by hydrogen bonds and hydrophobic interactions with an inherent nature of rigidity.

Mechanical tests showed that the stiffness of DN hydrogels increased dramatically when comparing to pristine hydrogels, and fast-reversible stiffness changes could be achieved within 1min by cyclic acid-base treatments. The CM-based DN hydrogel system also exhibited excellent shape fixing/recovering and self-healing efficiency. It showed time-dependent (acidic treatment) stiffness changes and self-healing property. As for the influence of the initial CM concentration, the stiffness changes were influenced by it on both the maximum value and increasing speed, while it didn't impair the self-healing efficiency suggesting a relatively stable self-healing ability.

The DN hydrogels with CNTs showed high sensitivity on capturing finger movements regardless of the moving speed. It could also be applied as a switch in electrical circuits exhibiting an "on-demand" ability. Another application as the LEGO-like 3D printing ink was demonstrated by the stepwise printing of required structures.

Taken together, this report provides a new strategy for the fabrication of multifunctional hydrogels based on the CM network.

1.5 Thesis Layout

This dissertation contains six chapters. The organization is as follows:

- Chapter 1 gives a brief introduction of background, problem definition, objectives, methodology and major findings;
- Chapter 2 presents a general literature review on hydrogel systems, stimuli-responsive bio-inspired hydrogel systems and recent advancement on CM-based hydrogels;
- Chapter 3 concludes detailed experimental procedures and used instruments;
- Chapter 4 expresses the results and discussion;
- Chapter 5 summarizes the major findings and conclusions of the whole research;
- Chapter 6 provides expectation and suggestion for future works.

Chapter 2

Literature Review

2.1 Hydrogels

Hydrogels are defined in many different ways by researchers ever since its appearance in 1960, one of the most commonly accepted description is that hydrogels are water-swollen materials (usually contain above 85% of water with the ability to absorb and retain more) and are formed by 3D like cross-linked polymeric networks through chain or step polymerizations (bulk, solution, suspension, emulsion). Their high water content endows them with good flexibility and makes them similar to natural tissues like human skins, organs, etc. Moreover, hydrogel systems are considered to be the most important extracellular matrix (ECM) analogs for tissue engineering and cell culturing. Due to their unique natural-like characteristics and the ability to integrate polymers with functional groups, enormous studies have been conducted in the past decades. Hydrogels have wild applications in biomedical areas like targeted drug vehicles[42], controlled drug release[43], tissue engineering matrices[44], etc., biotechnology areas such as bio-sensors with desirable flexibility, sensitivity and conductivity[45-47], separation technology areas such as oil-water filters[48], water purification[49], etc., agriculture industry such as nutrition controlled release of fertilizer-loaded hydrogels[50], cosmetic industry such as the use of Chitosonic®Acid. Based on the sources, cross-linking types, physical appearances, compositions and properties, hydrogels can be classified into different categories (Figure 1). Among these classifications, nanocomposite

hydrogels, hybrid hydrogels and double network (DN) hydrogels are of particular importance. Because sole hydrogel systems often suffer from weak mechanical properties and are hard to perform desirable functions due to the limitation of polymer modifications. Therefore, these hydrogel systems are introduced to not only improve hydrogels' mechanical performance but also bring functional features such as self-healing, shape-memory and reversible stiffness into one material.

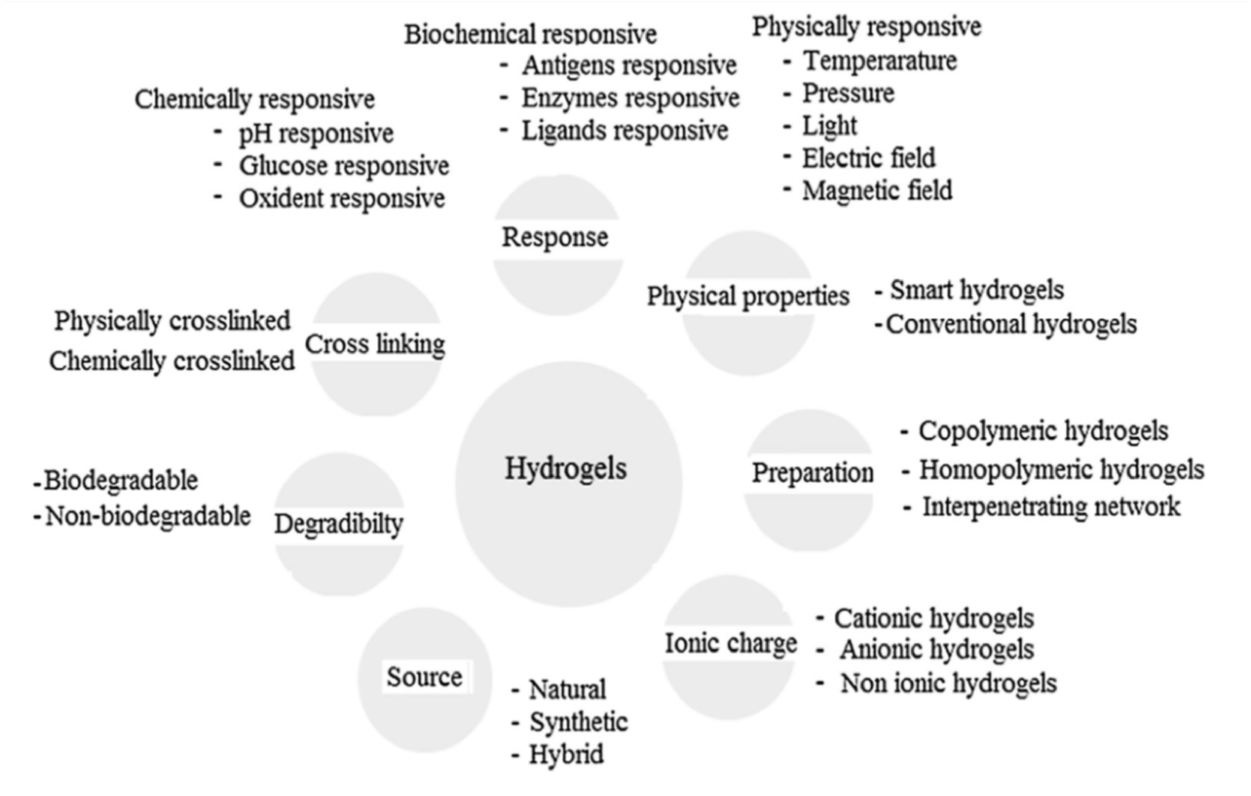

Figure 1 Hydrogel classifications fall into seven categories[51].

2.1.1 Nanocomposite Hydrogel Systems

Nanocomposite hydrogel systems are good fusions of nanotechnologies and biotechnologies. This combination offers great opportunities to fabricate materials with complex contents and desirable abilities and expends the applications into different areas. Hydrogels often possess interconnected pores (> 10 μm), and the pore sizes can be controlled by many ways such as solvent evaporation/infiltration and incorporation of non-cross-linkable polymers. The porous 3D structures of hydrogels enable them to absorb or incorporate molecules/polymers of nanoscales to show versatility. Generally, nanocomposite hydrogel systems are made through two ways: cross-linked hydrogels swollen in nanoparticles presented solvents or *in situ* gelation of polymers with the presence of nanoparticles[52]. The role of nanoparticles is essential to improve hydrogels' properties, they can be used by attaching to the polymer chains or by simply being entrapped in polymer networks. And these "additives" could improve hydrogels' physical properties such as enhanced mechanical performances, optical changes, magnetic/electric/thermal/UV responsiveness, etc. When comparing to the conventional hydrogels, nanocomposite hydrogels have improved empirical applications in biotechnology areas (Figure 2).

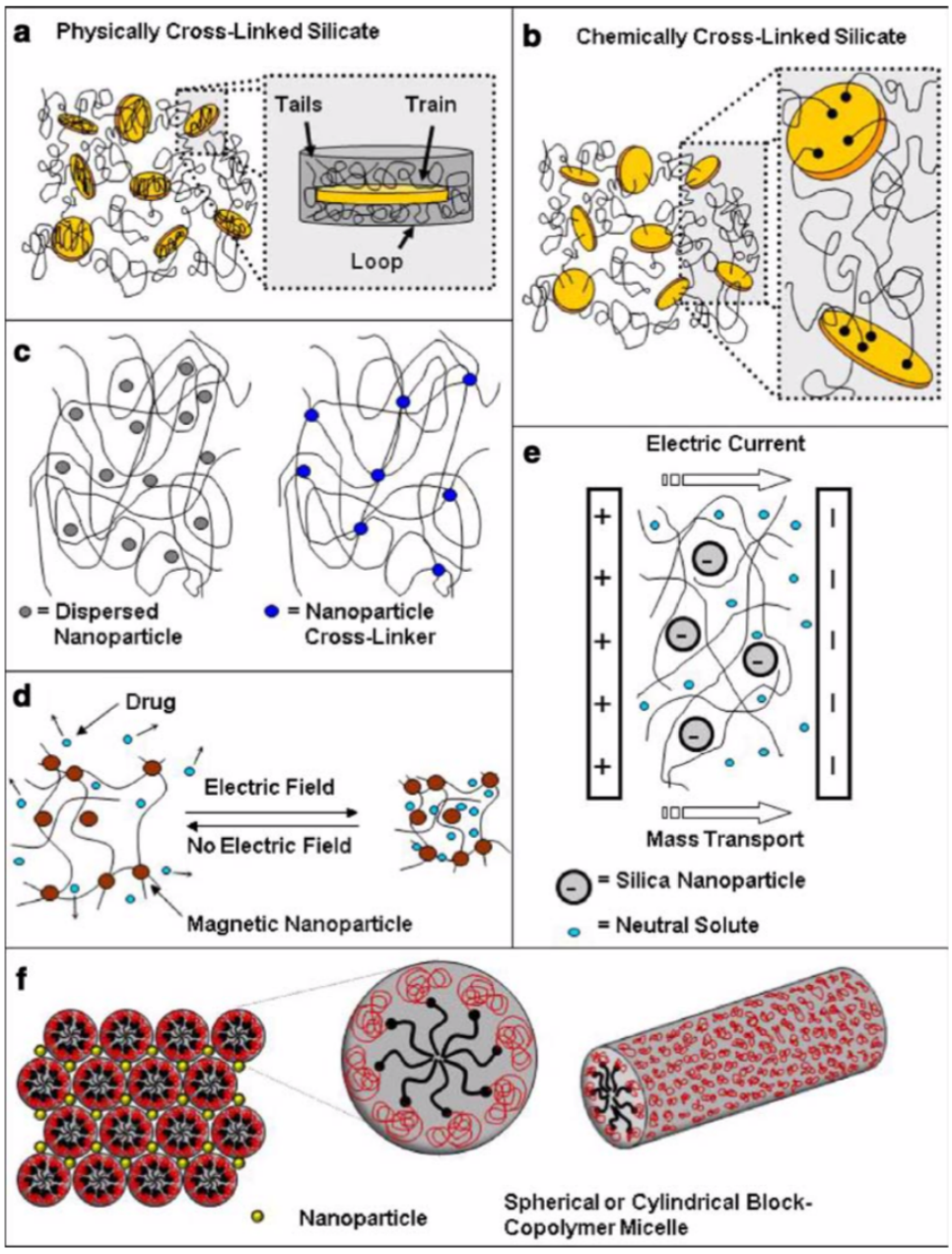

Figure 2 A general view of the applications of nanocomposite hydrogels[52].

To date, the most wildly used nanoparticles include clay, hydroxyapatite (HAp), and metallic nanoparticles. Montmorillonite (MMT), attapulgite and laponite have been employed into the constructions of clay nanocomposite hydrogels. Poly (N-isopropyl acrylamide) (PNIPAm) / clay nanocomposite hydrogels showed stimuli-responsive abilities and excellent mechanical performances. Furthermore, the properties could be tuned simply by altering the content of clay, and the clay-clay, clay-polymer interactions worked as "cross-linkers" to generate and reinforce hydrogels and bring self-healing abilities to the systems[53-56]. Natural polymers such as alginate and cellulose had also been utilized for clay nanocomposite hydrogels when combining with polyethylene glycol (PEG) [57-59]. Nanocomposite hydrogels can be fabricated into controlled release drug vehicles with a stable release throughout the whole releasing period[60].

Metallic nanoparticles include gold (Au), silver (Ag), iron (Fe^{3+}) and titanium (Ti). Different from clay nanoparticles, those metallic nanoparticles could afford the hydrogels with antibacterial abilities, magnetic and electrical properties. The processes of forming metallic nanocomposite hydrogels are normally in situ polymerizations of precursor solutions that contain metallic nanoparticles. Therefore, the particles are simply dispersed and entrapped within the networks of matrices. This kind of composites hydrogels is mostly used as biosensors[61], antibacterial wound dressings[62], etc. Hydroxyapatite (HAp) is the inorganic component of mammalian bone tissues, hence it has inherent biocompatibility and excellent biomimetic structures. In addition, the incorporation of HAp can significantly increase hydrogels' toughness and extensibility. PEG/HAp nanocomposite hydrogels were proven to have 5.07 MJ/m^3 toughness and 15.1 KPa elastic modulus which was 10 times and 5 times higher than that of pristine hydrogels (0.5 MJ/m^3 and 3.7 KPa)[63]. Taken together, hydrogels with nanoparticles involved can have ample uses in

biomedical areas and bring new branches in hydrogel's fabrication.

Tissue engineering and regenerative (TER) is introduced to repair, regenerate damaged tissues and organs, and it's attracted arising attention due to its importance in maintaining the functionality integration. Nanocomposite hydrogels in the field of TER often contain matrices that have controllable biodegradability. And they also have bioactive nanoparticles that can either help the matrices to remain stable in physiological conditions or improve the effectiveness of tissue engineering and regeneration[64]. For example, PEG/clay nanocomposite hydrogels were tested to have enhanced compressive and tensile properties than PEG hydrogels, yet they didn't impair the 2D cell adhesion, growth, spreading and the 3D cell encapsulation. Such nanocomposite hydrogels could have *in vivo* applications such as injectable scaffolds that have minimal invasion[57]. Chitosan/HAp scaffolds had also been evaluated to show similar mechanical improvements and enhanced biological properties[65]. Nanocomposite hydrogels can also be applied in drug delivery areas since the interactions among drug molecules, hydrogel matrices and nanoparticles can make them good reservoirs for delivering and releasing. Notably, thermal and pH-sensitive hydrogel systems are of major concern due to the gradually changing temperature and pH in the human body. And the addition of nanoparticles has bestowed the hydrogels with the ability to respond to external stimuli therefore empowering the accuracy and sensitivity of drug release. For instance, Serant et al. reported a graphene-based nanocomposite hydrogel that had "on-demand" drug release ability by responding to electro-stimulation[66]. Compared with conventional hydrogel systems, nanocomposite hydrogel systems exhibit superior mechanical and biological performances.

2.1.2 Hybrid Hydrogel Systems

The hybrid hydrogel system is generally considered as a system that contains multiple ($\geqslant 2$) components such as proteins, polysaccharides, PEG, poly (acrylamide) (PAM), peptide and more. And some components form the basic cross-linking structures, while the physical properties such as Young's modulus, strength, elasticity, diffusion are reinforced by the other components. For example, components like cell adhesion ligands, degradable polymers, signaling molecules or therapeutics are added into systems to improve biological activities. Therefore, hybrid hydrogel systems are usually used to edit hydrogels' functions and are extensively studied to have numerous applications[67].

The hybrid systems can be obtained through chemical reactions of various polymers, such as free radical polymerization of poly(ethylene glycol) diacrylate (PEGDA)/heparin methacrylate (HepMA) [68], click chemistry through Diel-Alder reaction[69] or thiol-yne chemistry[70]. The advantages of these methods are their fast reaction speed, highly specific reaction location, effective control of polymerization (initiating time, reaction duration, resultant molecular weight, etc.), and some of the networks may even have reversibility due to their reversible reaction mechanisms[24].

Physical interactions are another mean to construct hybrid hydrogel systems. Physical interactions often refer to hydrogen bonds, ionic interactions and hydrophobic interactions. Though the physical interactions often suffer from mechanical weakness and instability under external changes, the value of physical networks in hybrid hydrogels has been demonstrated[71-73]. Spontaneous self-assemble is one of the major applications of physical interactions. Hydrophilic and

hydrophobic polymers or molecules are used to construct amphiphilic polymers/molecules, after suspending them into solvents, the physical hydrogels can be formed.

The structures of physical hydrogels are determined by several parameters such as volume/weight percentages of hydrophobic/hydrophilic molecules, positions of molecules and properties of solvents, etc. Peptides are one of the most commonly used self-assembly macromolecules, and peptides conjugated polymers often possess both biological and mechanical properties[74]. Due to the complexity and difficulty in purification, natural polymers are often hard to modify. Therefore, natural polymer-based hybrid hydrogels are waiting to be further studied for biomedical uses. Biosynthetic elastin-like and resilin-like polypeptides are formed via recombination methods, which have proven to have better biological performances and controllable properties. For example, cell adhesion peptides were added to elastin-like polypeptides' sequences to improve cell culturing[75], domains with different functions (degradation enzyme, heparin-binding, etc.) were conjugated to polymers to exhibit the excellency out of both resilin and polymers[76].

Hybrid hydrogels are popular in biomedical fields because their properties can be altered by the variation of polymers/molecules at our wishes. Cell adhesion is considered to be the most critical factor in tissue engineering, yet many synthetic materials lack the ability to entrap cells. Cui et al. immobilized a short sequence of Arg-Gly-Asp tripeptide (RGD) onto the backbones of hyaluronic acid to form hybrid hydrogels. And it could promote neurites extension, support cell infiltration and angiogenesis, along with other enhanced biological performances when comparing with sole hyaluronic acid hydrogels[77]. Matrix metalloproteinases (MMPs) are a class of enzyme-sensitive peptides that are used to build hybrid hydrogels with desirable biodegradation actions. Chau et al.

inserted MMPs onto self-assembling blocks of the arginine-alanine-aspartate-alanine (RADA) to design novel bio-functional scaffolds with a similar biodegradation period as MMPs[78]. Other than these, hybrid hydrogel systems are also utilized in therapeutic studies such as tumor therapies and gene therapies. Qiu et al. reported a hybrid hydrogel system which was composed of gold nanorods and a thermally responsive hydrogel matrix with the loading of Doxorubicin, the release of drug was triggered by near-infrared lasers, and the hybrid hydrogel system significantly reduced tumor recurrence[79]. Short interfering RNA (siRNA) can silence gene expression to treat diseases, studies have shown that siRNA can be delivered when building a hybrid hydrogel by the thermosensitive polymer, and with the biodegradation and dissolution of the hydrogel matrix, the siRNA was released to perform antitumor effect *in vivo* for up to 4 weeks[80].

2.1.3 Double Network hydrogel systems

The interpenetrating network is one type of hybrid networks. The double network is one of the interpenetrating networks and is of importance due to its predominant mechanical strength. Double network (DN) hydrogels are normally made by two networks through separate polymerization steps, the first polymerization forms a tightly cross-linked network to provide enough mechanical strength and maintain integrity under damages and deformations, while the second polymerization forms a brittle and loosely cross-linked network which plays as the sacrificial role to effectively dissipate energy and/or bring other features to materials. Double network hydrogels are usually considered as mechanically tough hydrogels that contain fragile internal structures[81]. Figure 3 presents two charts for soft materials in terms of toughness and strength, and it can be observed that DN hydrogels have relatively high toughness with respect to fracture energy and mechanically

strong with respect to tensile strength. They are excellent candidates in biomedical fields such as cartilage repair and replacement, skin attached bio-sensors, etc.

Normally, DN hydrogels have one covalently cross-linked network through chemical reactions, and one non-covalently cross-linked network through hydrogen bonds, hydrophobic interactions, ionic interactions, etc. Sun et al. has reported a highly stretchable and tough hydrogel based on double networks[82]. The alginate and acrylamide were dissolved in deionized water as the precursor solution, then the photo-initiator, cross-linker and catalyzer for acrylamide, ionic cross-linker (calcium sulfate slurry, $CaSO_4 \bullet 2H_2O$) for alginate were added for polymerization. The DN hydrogels were tested to present extremely high stretching ability (beyond 20 times than their initial length) and toughness (fracture energies of ~9000 Jm^{-2}).

Different from this DN hydrogel that had with both chemical and physical bonds, Sun et al. designed versatile ionic combinations of polyampholytes by physical interactions between cationic polymers and anionic polymers[83]. They used polyampholytes with randomly dispersed cationic and anionic repeated units, some of them formed strong ionic bonds to serve as the permanent cross-links while others formed weak ionic bonds to dissipate energies by breakage of bonds. They synthesized the desirable polyampholytes from two aqueous solutions in which the monomers were at the opposite charging density, and they made the charging ratio to obtain approximately equal (1:1). The DN hydrogels contained less water (50-70wt%) than conventional hydrogels, strong viscoelastic and high toughness (4000 Jm^{-2}), along with 100% self-recovery and fatigue-free behavior. Notably, some hydrogels (NASS-co-MPTC) showed partial self-healing with a healing efficiency of 30% within 1h while the combination of (NASS-co-DMAEA-Q) could reach

to almost 100% after 24h. The authors envisioned that by the deliberate selection of the ionic combination, polyampholytes-based DN hydrogels could play a significant role in structural biomaterials.

In summary, DN hydrogels can significantly enhance hydrogels mechanical performances along with other functional features, and they are promising strategies in the construction of favorable hydrogels.

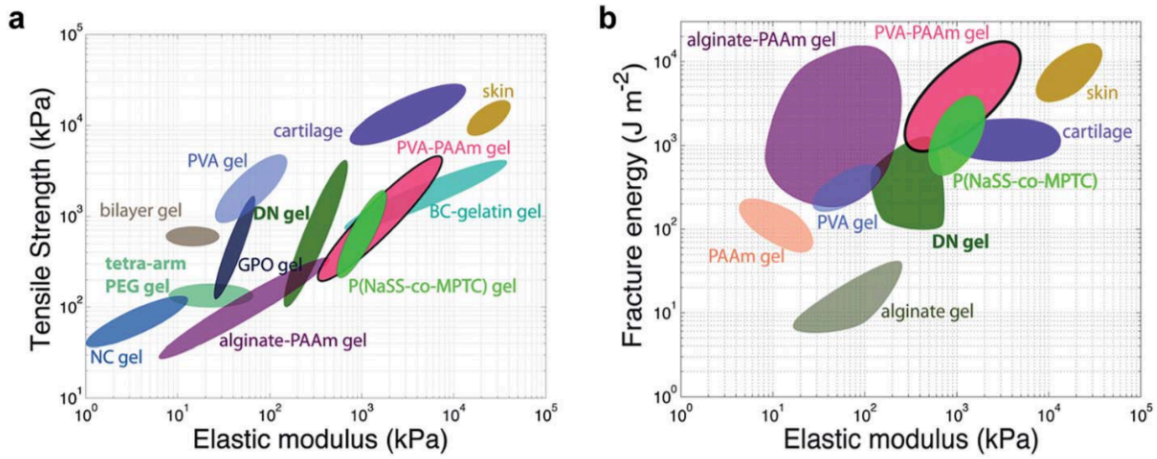

Figure 3 A general summary about material properties[84].

2.2 Bioinspired Stimuli-Responsive Hydrogel Systems

Nature is no doubt the foremost and best designer of all systems, biological models with outstanding traits that are fundamental for their survival are found throughout the whole history. Bioinspired materials with tunable or switchable properties have always been a great attraction due to their potential in the biomedical area, robotic area, electronic area, etc. Stimuli-responsive materials refer to materials that can alter their properties or performances in a predictable manner when responding to changes in the environment (i.e., pH, temperature, moisture, solvent, light, redox-reaction, catalyzer, etc.).Such materials are the mimicry to living organisms and have exciting prospects, and they are also categorized as smart/intelligent materials. Numerous efforts have been made to develop biomimetic materials, during which the exploitation of underlying mechanisms is of great value.

To date, various mechanisms including plasticizer-induced shape-memory, increased cross-linking density caused stiffness changes, self-healing by catalyzers are vastly investigated and utilized, yet more intriguing and straightforward means to achieve these desirable functions are still waiting to be explored. In spite of all differences among those mechanisms, one common similarity on the indicative facts is that either in natural systems or artificial systems, hierarchical structures and intricate interactions among components are key factors to realize such morphing. To take a glance at the development of the bioinspired stimuli-responsive hydrogel systems related to this project, hydrogel systems that have reversible stiffness, self-healing and shape-memory abilities are specifically reviewed in the following paragraphs.

2.2.1 Reversible Stiffness Change Hydrogels

Researches have proven that ECM's stiffness has a great influence on cell contractility, migration, spreading and differentiation[9, 10]. This phenomenon is mainly due to the responses from substrates to applied forces which in this case is the forces from cells. For example, on soft substrates, the cell deformation can be easily made without counterforce from substrates leading to weak cell responses, whereas the stiff substrates lead to higher molecular deformation thus activate further cell responses[85]. Similarly, stiff substrates enhance cell contraction[86], differentiation [10], migration[87], etc. Notably, ECMs *in vivo* are not always at the same condition, and they experience dynamic stiffness changes along with physiological changes. For example, the cardiac ECM stiffens after myocardial infraction impacting further differentiation. Thus, scaffolds, substrates and membranes with tunable stiffness have great potential in the biomedical area. Also, hydrogels with reversible stiffness can be employed as controlled release drug vehicles, environmental sensor, etc., due to their unique stimuli-responsive properties. Sea-cucumber-like reversible stiffness is one ideal model for the design of stiffness change hydrogels.

2.2.1.1 Sea Cucumber Dermis Model for Mechanically Morphing Changes

Many marine animals, especially echinoderms, such as sea cucumbers, sea urchins, etc., exhibit morphing with remarkable stiffness changes under threat. They can rapidly and reversibly alter the dermis tissue's stiffness (i.e., a contrast of elastic modulus of 5 to 50 MPa), which is considered to be their vital skill to survive. The root reason for this change is attributed to the regulation of interactions among collagen fibrils that are embedded in a viscoelastic matrix. Specifically, the dermis tissues of animals consist of abundant collagen fibrils that are inherently rigid, and the

surrounding tissues (ECMs) serve as the soft and highly elastic matrix providing conditions to trigger the stiffness changes by the mean of secreting stiffening agents (glycoprotein stiparin). The stiffening agents can bridge the disconnected collagen fibrils to form a load-bearing network. The reversibility of stiffness is achieved by sequential secretion of stiparin and its inhibitor (another glycoprotein that can competitively bind with stiparin to eliminate the stiffening effect by disassembling collagen aggregation)[88, 89]. Although the depth of underlying mechanisms of stiffness changes in sea cucumbers is not fully excavated, the idea of percolating stimuli-responsive rigid networks into soft matrices has been adapted into the construction of mechanically adaptive hydrogels.

2.2.1.2 Sea Cucumber-like Hydrogels

Christoph Weder's groups had firstly designed a serial of mechanically adaptive materials by using polymer nanocomposites to create similar architectures and properties as sea cucumbers[90]. They chose cellulose nanofibers to be the "collagen" in the materials owing to their high stiffness, strength, aspect ratio at the nanometer scale and economic-efficiency. More importantly, the numerous hydroxyl groups in the backbones of cellulose provided the possibility to regulate cellulose aggregation via hydrogen bonds. Ethylene oxide-epichlorohydrin (1:1) copolymer (EO-EPI) was firstly utilized to be the rubbery matrix due to its softness and solvent uptake ability. The cellulose nanofibers were incorporated within EO-EPI matrix through solution casting from dimethylformamide (DMF), and they served as the "whiskers" to reinforce hydrogel's stiffness at cues. The nanocomposite hydrogels containing 19% v/v whiskers exhibited dramatic stiffness improvement to 800MPa from 3.7MPa. And they ascribed this change to whiskers aggregation

due to the strong hydrogen bonds between hydroxyl groups.

Based on the understanding of the mechanism, they assumed that a good dispersion of whiskers could significantly moderate the inter/intra-molecular hydrogen bonds, therefore, softened the materials. Sulfate surface groups were introduced to cellulose whiskers to improve their dispersion in chemical solvents. By absorbing surrounding solutions, the whisker-whisker interactions were "switched off" through competitive hydrogen-bonding between whiskers and solvents to reduce material stiffness, whereas, upon evaporation of solvents, the whisker-whisker interactions were "switched on", therefore, a percolating network with reinforcement effect was formed. This stimuli-responsive mechanism was a mirror to that of the sea cucumbers. The nanocomposites exhibited a reduction of more than 40 folds of tensile modulus from 800 to 20 MPa at swollen equilibrium state. Isopropanol (IPA) was used as the reference solvent group to further confirm their mechanism. It could cause a similar swollen ratio as the water did while had no ability to disperse cellulose whiskers sufficiently. It turned out that at the same swelling degree the stiffness of nanocomposites in IPA experienced no reduction as those in water. This solidly suggested the reversible stiffness change was attributed to the aggregation and disconnection of cellulose whiskers through hydrogen bonds. Poly (vinyl acetate) (PVA)/cellulose whiskers nanocomposites were also fabricated to display similar reversible stiffness change with water as the regulator. They variated the solvent to artificial cerebrospinal fluid (ACSF), and the nanocomposites exhibited similar stiffness reduction within minutes. They continuously explored the use of cotton extracted cellulose whiskers as an alternative reinforcement component, investigated the possibility of using hydrophobic matrix and the effect of polarity of the polymer matrix[91-93].

Other approaches, such as using chitin-derived nanocrystals for mechanical property alternation were also studied[94]. What's more, the amino or carboxylic acid modified cellulose whiskers exhibited pH-induced reversible stiffness changes through a mechanism that was a bit different from the one discussed above (interactions reinforced by the removal of plasticizer)[95]. Figure 4 illustrates the mechanism of reversible stiffness change by modified cellulose whiskers.

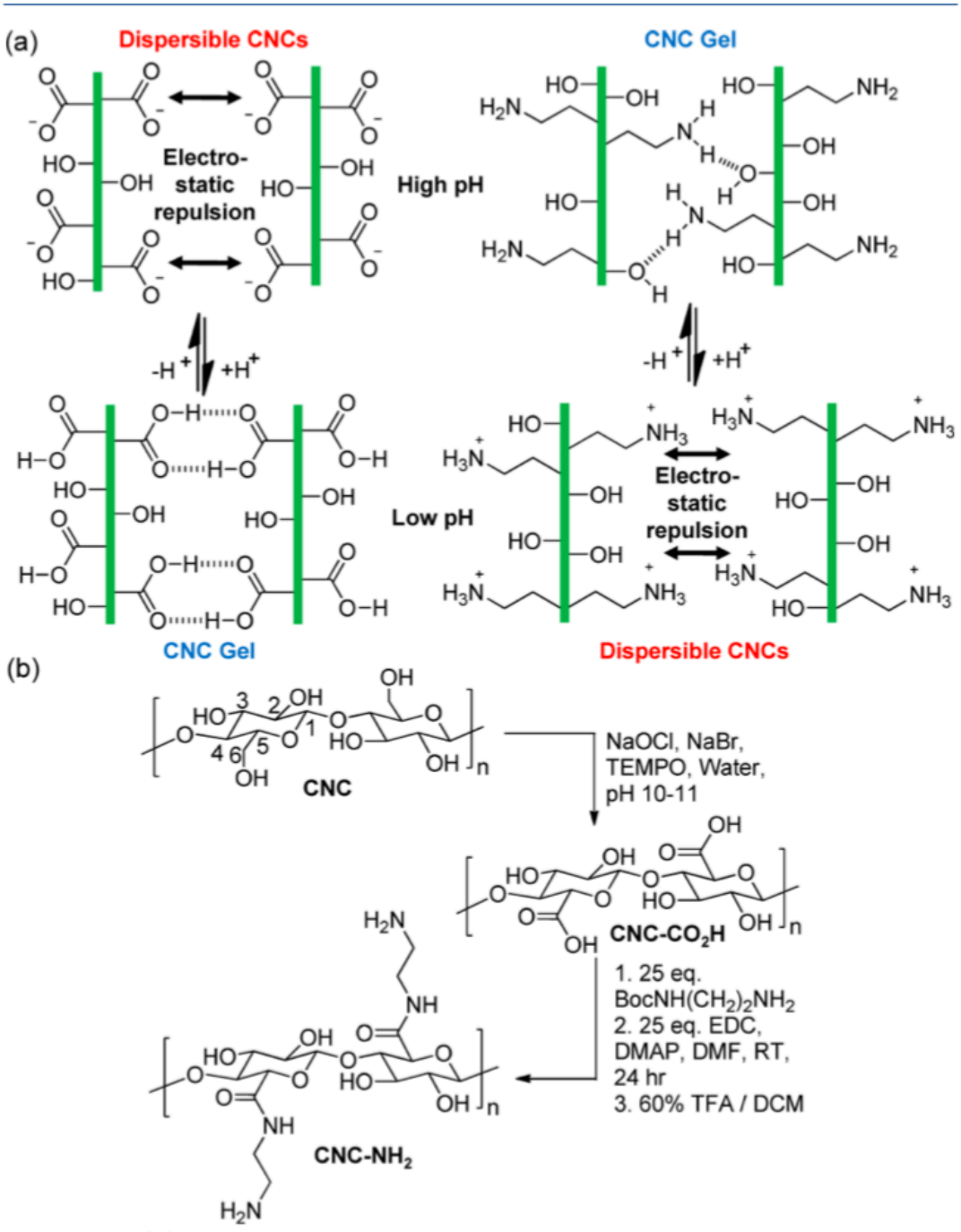

Figure 4 (a) Representation of the interactions between CNC−COOH and CNC−NH_2 at different pH; (b) Synthesis process[95].

2.2.2 Self-Healing Hydrogels

Self-healing is considered as one of the most remarkable abilities in biological organisms since it sufficiently maintains body integrity. Self-healing process involves two steps: the crack on the surface or inside, then autonomous or non-autonomous self-healing in the wounded sites. Self-healing in biomaterials is often caused by dynamic bonds either chemically or physically, and self-healing materials are classified into two categories: automatic self-healing materials and stimuli-responsive self-healing materials. The importance of self-healing ability in materials is that it not only prolongs materials' lifetime but also helps the materials to have uncompromised properties even after damages. Self-healing ability of materials is measured by several parameters including self-healing efficiency (mechanical robustness) and self-healing time (speed). Materials have high self-healing efficiency within short time periods are demonstrated to be applied as antifouling and antibacterial coatings[96], 3D cell encapsulation and drug delivery[24], tissue engineering[97, 98], etc.

2.2.2.1 Automatic Self-Healing Hydrogels

Automatic self-healing is defined as the kind of self-healing that happens automatically without external help. Hydrogels with automatic self-healing abilities are firstly investigated by macroscopic tests. For instance, cutting an integrate hydrogel into halves, and the hydrogels can heal back together and withstand their weights after reattachment of surfaces for a certain time. More comparative tests such as tensile or compressive tests and the elongation comparison tests are often used to determine self-healing quantitatively. Rheological experiments are also used to confirm automatic self-healing hydrogels, the cross-points of storage modulus (G') and loss

modulus (G'') are often used as an indication of sol-gel transitions and should be observed in all automatic self-healing hydrogels. Moreover, the continuous strain sweep tests are used to quantify hydrogels' self-recovery ability which reveals the reversibility of internal network upon damage. Normally, physical cross-links exhibit 100% self-recovery while most of self-healing hydrogel systems show lower values due to the strong and irreversible chemical cross-links[99, 100].

Automatic self-healing often consists dynamic bonds including covalent bonding (acylhydrazone and disulfide bonds)[101], hydrogen bonding (tannic acid and GelMA)[102], ionic bonding (ferric ions and carboxyl acid groups)[103], hydrophobic interactions (hydrophobic surface aggregation in aqueous media)[104], etc. Despite the ample mechanisms, self-healing hydrogels which imitate natural mechanisms are rarely reported. Lee et al. reported an approach to mirror the mechanism in vascular blood clotting. They added nanoparticles to polymers and yielded self-healing materials[105]. In their study, the nanoparticles localized at cracks to mend damaged regions, the healed materials were evaluated to restore 75%-100% properties of the original materials. Another report presented targeted self-healing ability in micro-cracks by employing poly (ethyleneoxied)-covered 5.2-nm spherical nanoparticles in poly (methyl methacrylate) matrix[106]. However, these self-healings are limited in micro- or nano- scale cracks which hinder their applications in macro-levels.

Another mechanism in a similar fashion of "bleeding" is also utilized in the design of self-healing hydrogels. White et al. incorporated a microencapsulated healing agent and its catalyzer within an epoxy matrix to build an automatic healing material[107]. In details, they used dicyclopentadiene (DCPD) as the healing agent due to its long shelf life, low viscosity and rapid polymerization

without apparent shrinkage. DCPD was firstly trapped in microcapsules made by urea-formaldehyde shells in order to separate catalyst and DCPD before the damage. When crack happened, the DCPD would release to the crack plane by capillary action, and then the polymerization of DCPD was initiated by transition metal catalyst (Grubbs' catalyst) at room temperature. The formed DCPD network was highly cross-linked and rigid which healed the crack sites yielding 75% of recovery of the fracture energy. To confirm their theory, materials without catalyst were fabricated as control groups which showed no ability to self-heal, which suggested that the self-healing phenomenon was caused by the formation of DCPD network. Their work constructed a new biomimetic self-healing concept.

2.2.2.2 Stimuli-Responsive Self-Healing Hydrogels

Another type of self-healing hydrogels is the stimuli-responsive ones in which the self-healing performance is realized by additives (i.e., light, pH, UV, chemicals, etc.). pH is one of the most commonly seen regulators for stimuli-responsive self-healing hydrogels. For example, He et al. reported diols-boronic acid complexation based self-healing hydrogels that self-healed at pH=9 and separated at pH=3[108]. The hydrogels were initially fabricated through interactions of poly (ethyleneglycol) (PEG) and 1,3-benzenediboronic acid. The stability of tetrahedral borate ester was highly dependent on the pH values, when pH was above the pK_a of diol, the cross-linking happened due to diol ionization while it de-cross-linked when pH was below pK_a. Although the authors didn't apply the quantitative measurement, the healing could occur within 30s, and the healed ones were able to be stretched a little. Another commonly seen type of hydrogels are redox-responsive self-healing hydrogels[109]. Ferrocene (Fc) derivatives are well-known redox-

responsive materials. After modifying poly (acrylic acid) (pAA) with Fc, the pAA-Fc was used as the guest polymer in a guest-host interaction with pAA-cyclodextrins (pAA-CDs). 14mM NaClO and 20mM glutathione (GSH) were chosen to be the oxidant and reductant, respectively. The hydrogels experienced sol-gel transitions with the addition of NaClO and GSH. The redox-responsive self-healing behavior was observed as follow: the hydrogel exhibited self-healing due to the reversible host-guest interactions, however, NaClO-treated hydrogels didn't show self-healing abilities, after spreading GSH onto the cutting surface the two separate parts adhered together. As shown above, the key factor of stimuli-responsive self-healing hydrogels is reversible cross-links that can be triggered externally and sequentially.

2.2.3 Shape-Memory Hydrogels

Shape-memory hydrogels are designed by mimicking the movement of animals like octopus or reactions of environment-sensitive plants like leaves' closing of touch-me-nots, blooming of flower petals. Scientists are inspired to create materials that have shape-memory properties due to their academic and industrial values. Materials with the ability to memorize a permanent shape, fix a temporary shape and relax to an original shape under thermal, chemical or environmental changes are considered to obtain shape-memory properties. The three phases of shape conditions allow the materials to be used as sensors, actuators, smart devices in the biomedical area[110, 111]. The most commonly used shape-memory materials are shape-memory alloys, but they suffer from poor elastic deformation and biocompatibility, high cost and labor wasting when comparing with shape-memory hydrogels. Shape-memory hydrogels are mainly used as biodegradable sutures[112], actuators[113-115], smart devices[116, 117].

2.2.3.1 Thermal-Responsive Shape-memory Hydrogels

Most of the shape-memory hydrogels are thermal-responsive, that is to say, the fixing of temporary shapes and recovery to memorized shapes are achieved through the manipulation of temperature. They usually consist of a soft matrix to perform deformation and a component whose structure can be controlled by temperature. The deformation shapes (temporary shapes) are usually made above (sometimes below) a critical temperature, then the temporary shapes are fixed by reducing or increasing the temperature below or above the critical temperature, finally, when the temperature is again across the critical point, the original (permanent) shapes are regained. The main reason for this transition is the stiffness changes between the heating and cooling cycles[118, 119].

One example is the thermally activated shape-memory hydrogels developed by Jinkun Hao and R. A. Weiss[120]. They designed a hydrogel system containing N,N-dimethylacrylamide (DMA), 2-(N-ethylperfluoro-octanesulfonamido) ethyl methacrylate (FOSM), hydroxyethyl acrylate, and 2-cinnamoyloxyethyl acrylate. The intricate interactions involved both physically and chemically, the nanodomains on FOSM molecules had a glass transition temperature which corresponded to the temperature used for the transition from temporary shapes to original shapes, in this case, the critical temperature was 65˚C. Interestingly, the mechanical properties of this hybrid hydrogel system could be simply altered by the variation of molecular compositions, i.e., hydrogels with higher a molar ratio of FOSM exhibited higher tensile modulus. The shape-fixing efficiency was achieved to be 88% after fixing at 10˚C for 24h and recover to ~100% of the original shape after heating up to the critical temperature.

2.2.3.2 Non-Thermal-Responsive Shape-memory Hydrogels

Other stimuli for shape-memory hydrogels are also developed such as light, chemical or other regulators[121]. To have a better understanding of the shape-memory mechanism induced in this project, mechanically adaptive shape-memory systems are reviewed specifically. The mechanically adaptive hydrogels can possess reversible stiffness changes upon external regulators, and their behaviors are detailed in the section of "Sea Cucumber-like Hydrogels". Since the transition between temporary shapes and permanent shapes require a significant difference of stiffness, the same mechanism should be able to apply on building shape-memory hydrogels.

In the presence of 20% v/v cotton cellulose nano-whiskers (CNWs), the tensile storage modulus (E') showed a reduction from 1GPa to 144MPa upon exposure to water which was in agreement with the previously illustrated mechanism due to the competitive hydrogen bonding. The high elastic nature of the matrix and the mechanically adaptive behaviors were the route reason for shape-memory ability. Briefly, the initial hydrogel was deformed into an intermediate shape after wetting, and then it was dried to get a stress-free temporary shape, finally the original shape was recovered by absorbing water and being dried again. The shape-fixing efficiency (F) and shape-recovery ratio (RR) increased as the CNWs' concentrations increased and hydrogels with 20% v/v CNWs showed 74.3% of F and a reasonable RR of 55.2%. On the other hand, the sole polyurethane (PU) showed poor shape fixing efficiency (13.3%) and relatively no shape recovery abilities (1.6%)[122]. Therefore, this mechanically adaptive mechanism provides a new general approach, and more types of shape-memory materials are yet to be exploited.

2.2.4 Multifunctional Hydrogels

As observed in nature, many living organisms can integrate multiple functions. For example, the dermis of sea cucumbers can not only exhibit reversible stiffness changes but also show self-healing abilities after damages. These combinations provide them with the ability to adapt to various situations. Therefore, designing materials with multi-functions becomes the ultimate goal effortlessly pursued by scientists. Although the fact that shape-memory abilities often come with stiffness changes, the confliction between the mechanisms of reversible stiffness changes and self-healing abilities has been a big barrier. For example, the ability to self-heal requires dynamic bonding such that is generally weak and can be easily broken and reformed, whereas these bonding cause poor mechanical strength. Hence, it is hard to get hydrogels with high stiffness out of these bonding.

Until today, rare studies have been reported on successfully obtaining hydrogels with multi-functions as mentioned above[31, 33, 123]. For instance, carboxymethyl cellulose (CMC) were functionalized with nucleic acid tethers and electron donors/acceptors, and the reactions between them were utilized for polymerization. The complexation of electron donors/acceptors could be separated by oxidation, and by cyclically applying oxidation and reduction, the hydrogel exhibited reversible stiffness changes which could be used to present shape-memory activities. Besides, the donor-acceptor units were also utilized to develop stimuli-responsive self-healing properties.

One common mechanism of these designs is that the hydrogel systems often consist dual cross-linking networks where one is cyclically generated/eliminated upon external stimuli and caused significant stiffness changes, while the other one provides stable and soft matrices during

processing. One of the disadvantages of recent developed multifunctional hydrogels is that the realization of as-desired functions is very complex. For example, CNC was modified several times to obtain desirable moieties, and complicated chemical conditions were used as stimuli. Furthermore, the stiffness changes were not as flexible and tunable as desired (only two stiffness levels). These disadvantages are going to be discussed and solved in this project.

2.3 Recent Advancement on CM-Based Hydrogels

2.3.1 Polysaccharide-based Hydrogels

Polysaccharides are important sources for biomaterials due to their good biocompatibility, controllable biodegradation, non-toxicity and biological activities originated from saccharide units. Many natural polysaccharides including alginate[124], chitosan[28, 125], gelatin[126], cellulose[127] and hyaluronic acid[128, 129] are wildly used as hydrogels in biomedical fields.

2.3.2 Current Advancement on Chitosan-based and CM-Based Hydrogels

Chitin is abundantly found and extracted from crustacean shells like shrimps, and chitosan is one derivative of it with linear polysaccharide structure[130]. Typically, chitosan has more than 60% of ß (1,4)-D-glucosamine residues and randomly located N-acetyl-glucosamine units (Figure 5). In neutral or basic aqueous solutions, the semi-crystalline and crystalline microstructure of chitosan makes it insoluble, however, in acidic environments, the amino groups are protonated into positively charged units which significantly increases its solubility. Notably, other than other polysaccharides, chitosan is the only naturally cationic polymer, the positive charge density

endows it with the ability to form ionic complexed with anionic polymers such as glycosaminoglycan (GAG), poly (acrylic acid)[131, 132].

Specifically, since the GAGs can interact or even directly link to a large number of growth factors, proteins, and lipids in the human body, chitosan-based biomaterials possess singular exploitable value. In the perspective of biomedical areas, considerable studies have been conducted on the applications of chitosan such as implants for tissue engineering and regeneration[133], pH-sensitive drug release cargos[134]. However, the poor water solubility has become its "Achilles' Heel", hence attentions have been shifted to the derivatives of chitosan that have good water solubility. Carboxymethyl chitosan (CM) is one of its derivatives that has received wild recognition, and its chemical structure is illustrated in Figure 5. Normally, the carboxylation of chitosan happens on either C6 or -NH2 based on the reaction conditions (i.e., alkalization time, solvent, temperature, etc.), and the degree of substitution has a great impact on the properties[135, 136]. Despite the extensive studies on CM-based hydrogels, they are mainly used in hybrid hydrogel systems to perform pH-sensitive drug release or as wound dressings when chelating with ions, yet the ability to form multifunctional double network hydrogels has not been reported[132, 137-139].

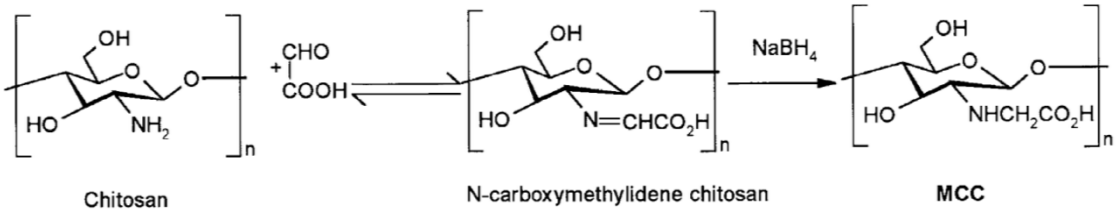

Figure 5 Schematic representation of the synthesis of the mono-N-carboxymethyl chitosan (MCC)[140].

Chapter 3

Experimental Procedures

3.1 Introduction

In this chapter, detailed experimental procedures of this project in this dissertation are concluded. In section 3.3, the preparations of different hydrogels are described along with the characterization procedures by FT-IR, ^{1}H NMR and SEM. In section 3.4, confirmation and evaluation methods for multifunctionality are described. Section 3.5 shows the potential applications for this hydrogel system.

3.2 Materials

Carboxymethyl chitosan (CM) (degree of deacetylation 96.1%, degree of substitution 82%) was purchased from Xi'an Lyphar Biotech Co., Ltd., China. Acrylamide (AM) was purchased from Aladdin Industrial Corporation (Shanghai, China). N, N'-Methylenebis(acrylamide) (MBA), Ammounium persulfate (APS) and N, N, N, N'-Tetramethylethylnendiamine (TEMED) were purchased from Sigma-Aldrich. Hydrochloric acid was purchased from Anachemia. Sodium hydroxide was purchased from Fisher Scientific. 1.5mL polypropylene microcentrifuge tubes were purchased from NEPTUNE. All agents in this study were used as received without further purification.

3.3 Preparation and Characterization of CM-Based DN Hydrogels

3.3.1 Preparation of CM Hydrogels

Firstly, the CM precursor solution containing 5% (w/v) CM was prepared. In details, 0.5g CM was added into 10mL deionized (DI) water, and then the mixture was vigorously shaken until a homogeneous solution was obtained. The gelation of CM hydrogel followed a lab-based protocol. Briefly, a certain amount of CM precursor solutions were moved to desired containers by pipette, in this case, the lids of 1.5mL polypropylene microcentrifuge tubes were used, and each of them could contain 200μL CM precursor solution. Then the containers with CM precursor solutions were placed under -20˚C until fully frozen. The frozen CM precursor solutions with specific shapes were taken out and immersed in 0.1M HCl solutions. After 10 min, the CM hydrogels were formed.

3.3.2 Preparation of AM Hydrogels

The AM hydrogels were prepared in a well-established way. A certain amount of AM was dissolved in DI water, then APS, MBA and TEMED were added to form gels. In details, 1.8g AM was dissolved in 10mL DI water to reach a concentration of 18% w/v, thus the AM precursor solution. Then, 500μL AM precursor solution was moved into 1.5mL centrifuge tube and 15μL APS (200mg/mL), 30μL MBA and 10μL TEMED (10%, v/v) were added, and then the mixture was mixed by Vortex Mixer for 5 seconds, the gelation was realized within 15 seconds.

3.3.3 Preparation of Pristine Hydrogels

The precursor solution for pristine hydrogel was made by AM, CM and DI water. 0.5g CM, 1.8g

AM were dissolved in 10mL DI water and then vigorously mixed until homogeneous to reach concentrations of 5% w/v and 18% w/v, respectively. Then the gelation of AM happened following the same protocol described in the preparation of AM hydrogels (the precursor solution : MBA : APS : TEMED = 500: 15: 30: 10).

3.3.4 Preparation of CM-Based DN Hydrogels

The preparation of the precursor solution for CM-based DN hydrogel was approximately the same as that of the pristine hydrogels. Briefly, 0.1g/0.3g/0.5g CM, 1.8g AM were dissolved in DI water to obtain a homogeneous solution with 1/3/5% w/v and 18% w/v of CM and AM, respectively. The construction of CM-based DN hydrogels was as follow: firstly, the gelation of pristine hydrogels; then the pristine hydrogels were incubated in acidic solutions for designed duration therefore achieving the construction of DN hydrogels. The CM-based DN hydrogels were described as DN-*x*-*y*, where *x* represented the acidic incubation time, and *y* represented the initial CM concentration. Unless otherwise noted, DN hydrogel(s) represented DN-30-5%, and 0.1M HCl, 0.3M NaOH were used to perform functional experiments.

3.3.5 ^{1}H NMR Spectra

The ^{1}H NMR experiments were conducted on Bruker Avance 300MHz NMR spectrometer, and the relaxation delay (d1) was set to be 2 seconds. CM was dissolved in D_2O to a concentration of 10mg/mL. The results were used to analyze the structure of CM with a specification of localizing the position of carboxylation.

3.3.6 FT-IR Characterization

Fourier transformed infrared (FT-IR) spectra were used to characterize the change of $-COO^-$ groups after acidic incubations in order to confirm the generation of the CM network. The FT-IR images were studied using Thermo Nicolet iS FTIR spectra, resolution of 4 and 64 scans per sample, and data were collected and analyzed by OMNIC software.

3.3.7 Scanning Electron Microscopy (SEM) Imaging

The formation of the CM network was further confirmed by scanning electron microscopy (SEM) images. Different types of hydrogels were prepared, i.e., CM hydrogels, AM hydrogels, pristine hydrogels, DN hydrogels, as well as DN-1-5%, DN-5-5%, DN-15-5%, DN-30-1% and DM-30-3% hydrogels. All hydrogel samples were frozen by immersing in liquid nitrogen for 5min and lyophilization. The lyophilized samples were broken into halves, and the halves were placed onto a metal sample holder with the cutting surfaces facing up, and a thin layer of gold was sputtered coated onto the surfaces. Then the images were obtained by Quanta FEG 650 with an operating voltage of 10kV. The pore sizes of each sample were analyzed by Image J software.

3.3.8 Swelling Ratio Tests

Swelling ratio tests were also conducted as an auxiliary method to prove the generation of CM networks. Cylindrical hydrogels with 8mm and 4mm of diameter and thickness were prepared for swelling ratio tests. The initial weights of AM gels, CM gels, pristine gels and DN gels were recorded as W_0, and then the gels were incubated in 20 mL DI water at room temperature, and the

DI water in each incubator was changed and refilled to the same amount every day. The W_t of gels after predetermined times were measured and the swelling ratio (SR) was calculated as: $SR(g/g) = (W_t - W_0)/W_0$.

3.3.9 Rheology Characterization

Rheology tests are broadly used in the section of preparation and characterization of DN hydrogels, reversible stiffness changes and self-healing. Here is the introduction of detailed procedures for each part. All samples were made into cylindrical shapes with diameter and thickness of 8mm and 4mm, respectively, and were tested on TA Discovery Hybrid Rheometer at 25˚C with an 8mm diameter parallel plate. In the preparation and characterization of DN hydrogels part, oscillatory frequency sweep tests (0.1 rad s^{-1} to 100 rad s^{-1}) at a fixed deformation strain of 0.01 were conducted for all samples. In the reversible stiffness section, the G' and G'' of DN-1-5% hydrogels were tested at a fixed angular frequency of 10 rad s^{-1} and strain of 0.01 during 100s, then the DN-1-5% hydrogels were incubated into basic solutions (0.3M NaOH) for another 1min, and the same rheological experiments were conducted. Three consecutive cyclical acid-base treatments were applied, and G' and G'' values of hydrogels after each treatment (acid or basic) were collected. In the self-healing section, the pristine hydrogel cylinders were tested by strain amplitude sweep tests at the strain range of 1% (small) - 700% (large) at a fixed frequency of 10 rad s^{-1}.

3.4 Multifunctionality Tests

Tensile and compressive results were used to measure the maximum stiffness changes and self-healing efficiency, while compressive tests were carried out to further investigate the stiffness

changes including influence factors and fast-reversible stiffness changes. Shape-memory abilities were determined by shape-fixing efficiency and shape-recovery ratio.

3.4.1 Sample Preparations

All samples for tensile tests were made to rectangle shapes with 10mm, 30mm and 2mm in width, length and thickness, respectively. In the section of maximum stiffness changes, three groups of samples including AM hydrogels, pristine hydrogels and DN hydrogels were tested. In details, 500μL of specific precursor solutions were moved into 1.5mL microcentrifuge tubes, then after adding certain amounts of APS, MBA and TEMED, the solutions were immediately poured into rectangular containers with as described dimensions to gel. The pristine hydrogels were then incubated in acidic solutions for 30min to obtain DN hydrogels. As for hydrogel's self-healing performances, hydrogels with the same shapes as those in testing stiffness changes were made. DN hydrogels with different initial CM concentrations and under various acidic treatment times were prepared. For the preparation of self-healed hydrogels, the pristine hydrogels were cut into halves, then two halves were reconnected through cross-section surfaces attaching, and they were incubated into acidic solutions for predetermined times.

All samples for compressive tests were made into cylindrical shapes with 8mm and 4mm of diameter and thickness, respectively. The gelation protocols were as described, the acidic incubation times for DN hydrogels were 1min, 5min, 15min and 30min, and the different acidic solutions used were 0.1 and 0.3 M HCl. To test the reversibility of stiffness changes, cylindrical hydrogels were incubated into acid/base solutions sequentially for cyclic treatments, each treatment (acid or basic) lasted for 1min, and hydrogels after each treatment were put under

compressive tests.

All samples for either tensile or compressive tests were coated with silicone oil to prevent water evaporation.

3.4.2 Macroscopic Tests

In the section of reversible stiffness changes, pristine hydrogels of rectangular shapes were lifted by a tweezer in the middle, then after incubating in acid for 1min, the obtained DN-1-5% hydrogels were again lifted by a tweezer in the same way. Finally, the DN-1-5% hydrogels were incubated in base for another minute followed by the same lifting action.

In the section of shape-memory abilities, pristine hydrogels of rectangular shapes (10mm, 10mm, 2mm in width, length and thickness) were elongated to twice their original lengths and incubated in acidic solutions for 1min to fix the shapes, then they were placed in sealed containers for 3h to calculate shape-fixing efficiency, finally, they were incubated in basic solutions for another 1min to recover. The lengths, widths, thicknesses and weights of hydrogels were recorded and calculated to evaluate the shape-fixing efficiency and shape-recovery ratio. Other macroscopic experiments were concluded as follows: the pristine hydrogels were dyed in red and made into different shapes (V modes and square modes), then the “V”s were twisted whereas the squares were expanded and incubated in acid and base for 1min sequentially.

In the self-healing section, the rectangular shapes pristine hydrogels were cut with a small wedge in the middle, then the separated parts were placed together and treated with acidic solutions for 1min, basic treatments were applied sequentially. Similarly, the pristine hydrogels were made into

two “half-heart-like” shapes, and one “half-hearts” were dyed in red for visual convenience, the linear areas of these two “half-hearts” were contacted and treated with acid and base for 1min sequentially.

3.4.2 Tensile and Compressive Tests

All mechanical tests were executed on INSTRON 5965 universal testing machine. For tensile tests, all groups of samples were tested by utilizing a 5KN load cell at a steady stretching rate of 10mm/min until break. For compressive tests, samples were tested by using a 1KN load cell at the same compressive rate as the tensile tests until break or to a maximum strain of 90% due to the limitation for the safe use of the machine. The tensile elastic modulus and compressive modulus were calculated by using the linear regions at initial stages of all tests (1%-10%) from stress-strain curves.

3.4.3 Statistic Analysis

All results are presented in mean ± standard deviation (SD).

3.5 Potential Applications

3.5.1 Sample Preparations

The precursor solutions for motion sensing and “on-demand” switch contained 5% CM w/v, 18% AM w/v and 1% CNTs w/v. To achieve a homogeneous dispersion of CNTs, the precursor solutions were subjected to ultrasonic treatments at ambient condition for 1h prior experiments.

Rectangular hydrogel strips were made for motion sensing and “on-demand” switch tests with the length, width and thickness of 20mm, 10mm and 2mm, respectively. CNTs-incorporated pristine hydrogels were incubated in acid solutions for 1, 2 and 3 min, respectively.

To reach high viscosity that was suitable for 3D printing, 1.8g AM and 1.8g CM were added in DI water and the mixtures were placed on a hot plate under 60˚C overnight to attain homogeneous solutions with concentrations of 18% w/v and 18% w/v, respectively. The precursor solutions were then sealed in 15mL centrifuge tubes and stored at room temperature for further use. Before 3D printing, certain amounts of precursor solutions were mixed with MBA and APS at the same scale as mentioned and then added to 3D printing syringe to conduct 3D printing experiments.

3.5.2 Motion-Sensing and “on-demand” switch

The resistances of hydrogels were measured by VICTOR 86E DIGITAL MULTIMETER. Two ends of the rectangular CNT-incorporated pristine hydrogels were connected to conductive copper wires and then sealed with polydimethylsiloxane (PDMS) films which acted as insulators and prevented water evaporation. The device was then placed onto the rear joint of the index finger, and the motion-sensing was recorded by the digital multimeter for real-time movement, data was collected and analyzed by DMM Data Processor.

The rectangular CNTs-incorporated pristine hydrogels were curved to a degree of 90˚ from the middle, and the shapes were fixed by incubating in acid for 1min. An open circuit was formed by a DC Power Supply QW-MS3010D, conductive wires, a light-emitting diode (LED) bulb and two conductive copper strips which were placed with distance (20mm gap), the hydrogels with fixed

shapes were then placed between the gap with one end attached to one of the copper strips. Then one drop of the base was applied on the surface of the curvatures.

3.5.3 “LEGO-Like” 3D Printing Ink

The DN hydrogel system could be applied as a “LEGO-like” 3D printing ink following a step-wise procedure: printing, gelation, assembling. In details, the complicated objectives were firstly divided into simple ones such as circles, triangles, squares, rectangles, etc. Simple codes were designed by G-code. After printing, drops of TEMED were applied on the spare space of the substrate and covered with a lid immediately for 10min. Specific parts of simple shapes were attached and treated with acid for 1min. The 3D printing process was operated via GEEETECH LCD2004 Controller with 60psi air pressure at the nozzle speed of 2mm/s on a glass substrate.

Chapter 4

Results and Discussions

4.1 Introduction

In this chapter, results and discussions of previously described experiments are presented. Section 4.2 shows the ^{1}H NMR, FT-IR and SEM results to characterize CM-based DN hydrogels, and the results of gelation, swelling ratio and rheology tests are also presented and discussed. In section 4.3, three functions of this hydrogel system including reversible stiffness changes, self-healing and shape-memory are investigated from macroscopic tests to mechanical tests and specific characterization methods are used and discussed to show its superiority. In section 4.4, three concept studies are presented and discussed to show its potential in applications such as biological motion sensors, "on-demand" switches and LEGO-like 3D printing ink.

4.2 Preparation and Characterization of CM-Based DN Hydrogels

4.2.1 Preparation of CM-Based DN Hydrogels

CM hydrogels were obtained followed by the procedure mentioned in 3.1.1. Notably, since CM molecules interacted with protons rapidly, our lab-based method was so far the best way to develop homogeneous cross-linking. As shown in Figure 6a, after 10min' immersion in the acidic solution, the fully gelled CM hydrogel appeared a spherical shape. It was assumed that this shrinkage

happened because the hydrogen bonding and hydrophobic interactions during the gelation process formed strong compaction forces along. Figure6 b-e show the outlooks of AM, pristine, DN hydrogels and DN hydrogels after basic treatments for 1min. Interestingly, AM and pristine hydrogels showed good transparency, whereas the CM hydrogels appeared opaque and DN hydrogels were translucent. Moreover, the color of DN hydrogels could be tuned by cyclic acid-base treatments (Figure 6d-e). Furthermore, the CM hydrogels were brittle, and the AM hydrogels and pristine hydrogels showed good elasticity (Figure6 f). The mechanical properties of DN hydrogels will be discussed thoroughly in 4.3.1.

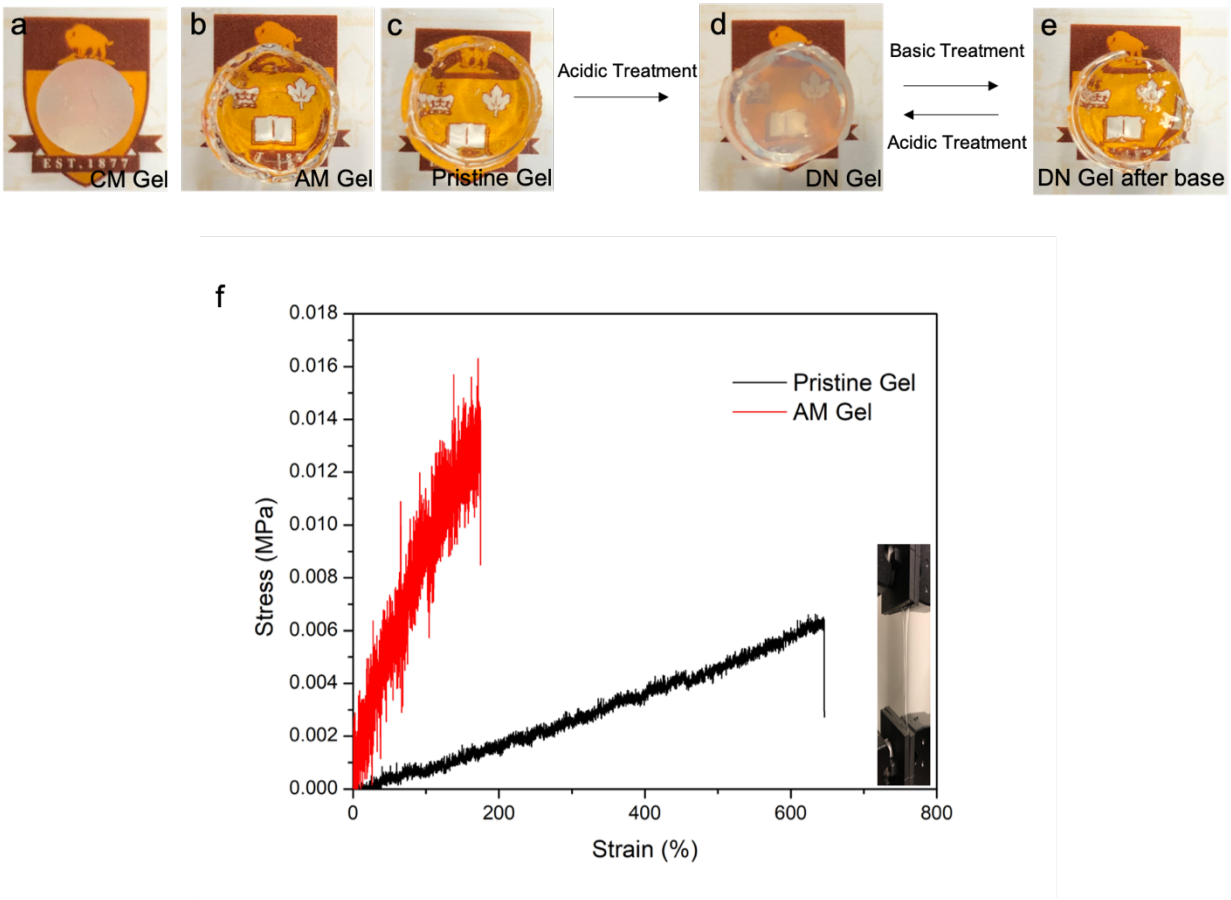

Figure 6 Photographic images of a) CM hydrogel, b) AM hydrogel, c) Pristine hydrogel, d) DN hydrogel and e) DN hydrogel treated with base for 1min. f) Tensile curves of pristine and AM hydrogels, insert is the photo of tensile tests.

4.2.2 Characterization of CM-Based Hydrogels

As mentioned in the literature view section, the CM is the carboxylation derivative of chitosan, and the substitution often happens on the C6 or N2 positions. The product provider had illustrated that the CM used in this project was N-carboxymethyl chitosan, ^{1}H NMR spectra was conducted to further confirm the chemical structures of CM molecules. As shown in Figure 7, it showed a typical CM resonance. The broad resonance peaks in the region of 3.3-4.0 ppm was ascribed to the protons conjugated on the saccharide rings that were overlapped, the peak of H-1 which was the hydrogen bonded to the anomeric carbon lied in the region of 4.4-5.0 ppm and overlapped with the solvent resonance on 4.8 ppm. The small resonance peak at 2.0-2.2 ppm was caused by the small amount of remaining acetamide. The sharp single peak at 2.4 ppm was assigned to the N-substituted $-CH_2COO^-$ groups, and the peak near it was the resonance of protons on C_2[141, 142]. Therefore, the ^{1}H NMR spectra have strongly proved that this CM is the N-carboxymethyl chitosan. Since it has 96.1% degree of deacetylation and 82% degree of substitution, and there's no obvious resonance peak observed in the region of 4.0-4.4 ppm which is ascribed to $-O-CH_2COO^-$ groups, there's little residual $-NH_2$ groups in this CM and approximately all of them are substituted with -CH2OO$^-$ groups.

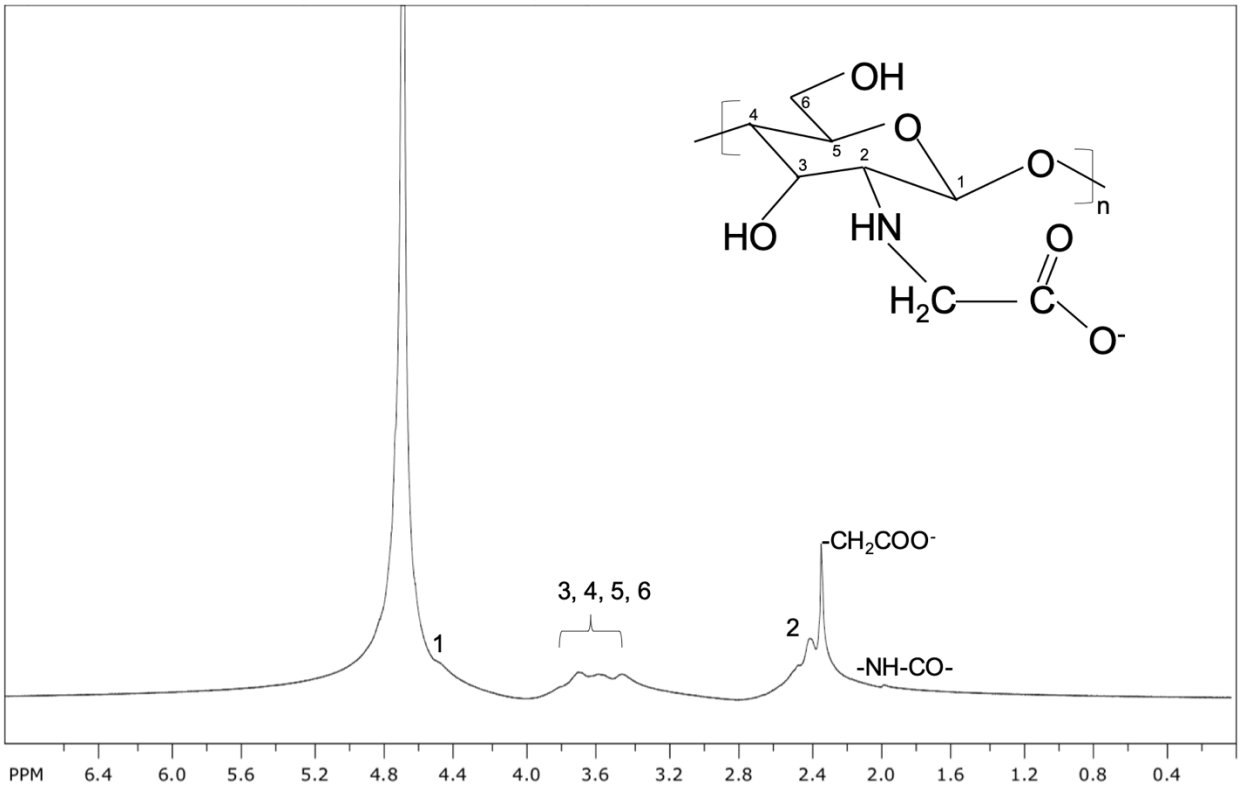

Figure 7 [1]H NMR spectra of CM molecules.

Hence, the underlying mechanism of the gelation of CM is as follow: when absorbing protons, the $-COO^-$ groups on CMs were protonated to -COOH groups which would cause the screening of molecular electrostatic repulsion, therefore, the well-dispersed CM chains aggregated together and formed strong hydrogen bonds among secondary amino groups, hydroxyl groups and carboxyl groups, other than this, the protonation significantly impaired the water solubility of CM and caused strong hydrophobic association which in turn enhanced the entanglement of CM chains, these exquisite blends of synergetic interactions resulted in a stable and rigid physical CM network, and the elimination of this CM network could be obtained by deprotonation of -COOH groups. Notably, when the CM molecules were incorporated into a soft and stable matrix formed by networks like the PAM, the reversible generation and elimination of the CM network could bring intriguing properties to the DN system. The mechanism of CM-based DN hydrogel is schematically illustrated in Scheme1.

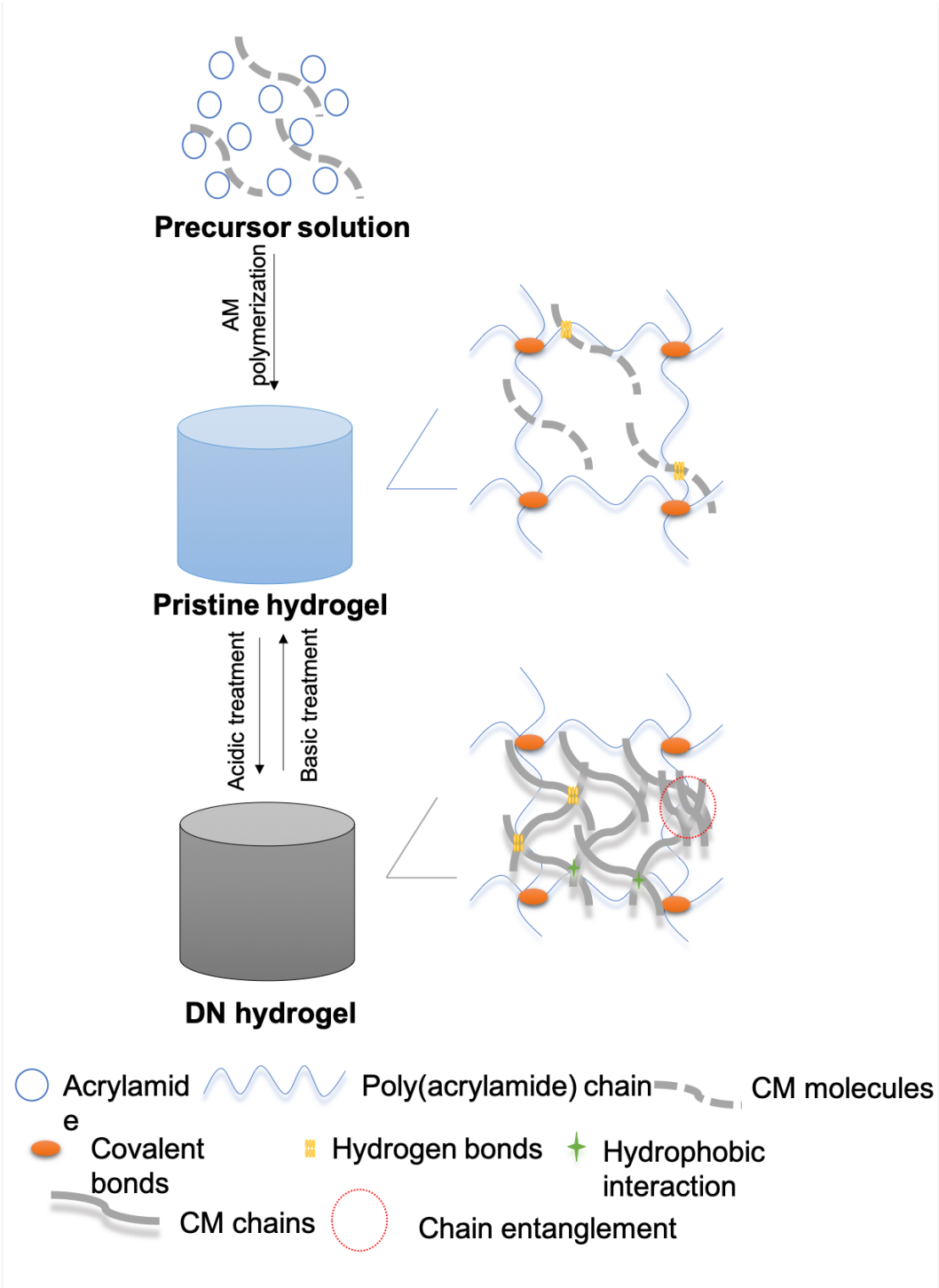

Scheme 1 Schematic illustration of the mechanism of CM-based DN hydrogel.

To further confirm this hypothesis about the conversion between -COO^- groups and -COOH groups, FT-IR experiments were carried out. The FT-IR spectra of CM and lyophilized CM gels were shown in Figure 8. It is easily observed that both of them showed featured bonds of chitosan derivatives in significant regions as follows: the broad spectrum lied in the region of 3000-3300 cm^{-1} stands for O-H bonds (stretching vibration) which overlapped with N-H bonds, and the peak at the region of 2850-2950 cm^{-1} was due to the absorbance of C-H bonds (axial stretching vibration), the peak at 1500-1700 cm^{-1} was ascribed to the stretching vibration of -C=O and N-H bending. Furthermore, the asymmetric and symmetric stretching vibration at 1549 cm^{-1} and 1429 cm^{-1} confirmed the existence of –COO^- groups in CM molecules while the strong absorbance at 1715 cm^{-1} indicated the appearance of –COOH groups suggesting the neutralization process after acidic treatments[135, 143, 144]. The FT-IR indicated the protonation and deprotonation of CM molecules, which confirmed our hypothesis and mechanism.

Swelling ratio tests were conducted to show the formation of CM network. Hydrogels are well-known for their high water content and good water absorption capacity, after water intake, most hydrogels exhibit isotropic expansion and weaker mechanical properties. However, the DN hydrogels exhibited much lower swelling ration than other groups with a swelling ration of 0.18 (SR(g/g)), and there was negligible volume expansion compared to other groups (Figure 9c-h). On the contrary, the swelling ratio for the AM and pristine gels were 7.3 and 4.9 (SR(g/g)) (Figure 9a-b), respectively, and they both exhibited obvious volume expansions. Notably, the CM gels had almost no water absorption (SR(g/g), 0.005) showing an inherent water-stability and water resistance, which should be the root reason for the much lower swelling equilibrium ratio of DN hydrogels. This further confirmed the formation of the CM network in DN hydrogels.

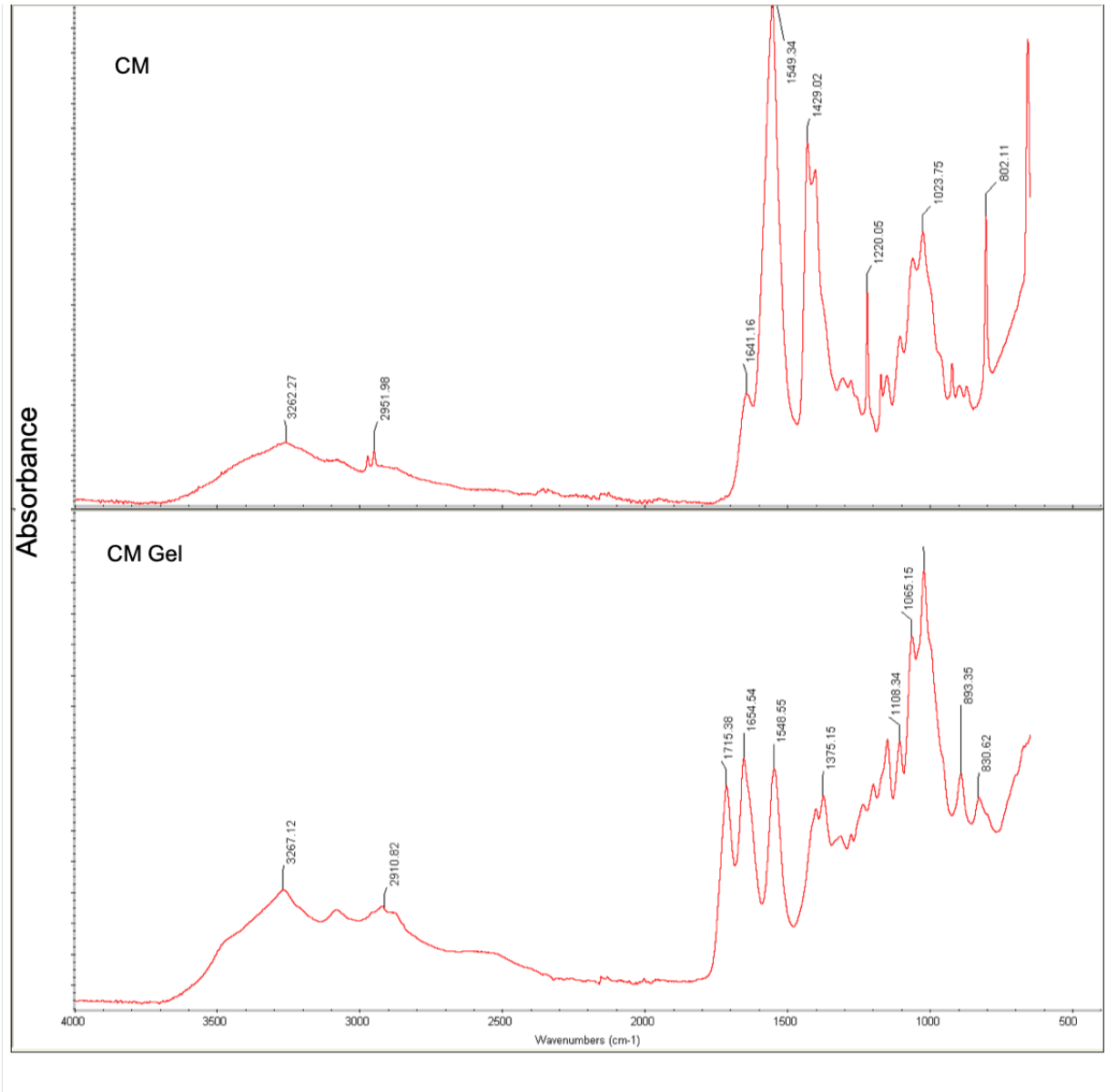

Figure 8 FT-IR images of (top) CM and (bottom) CM gel.

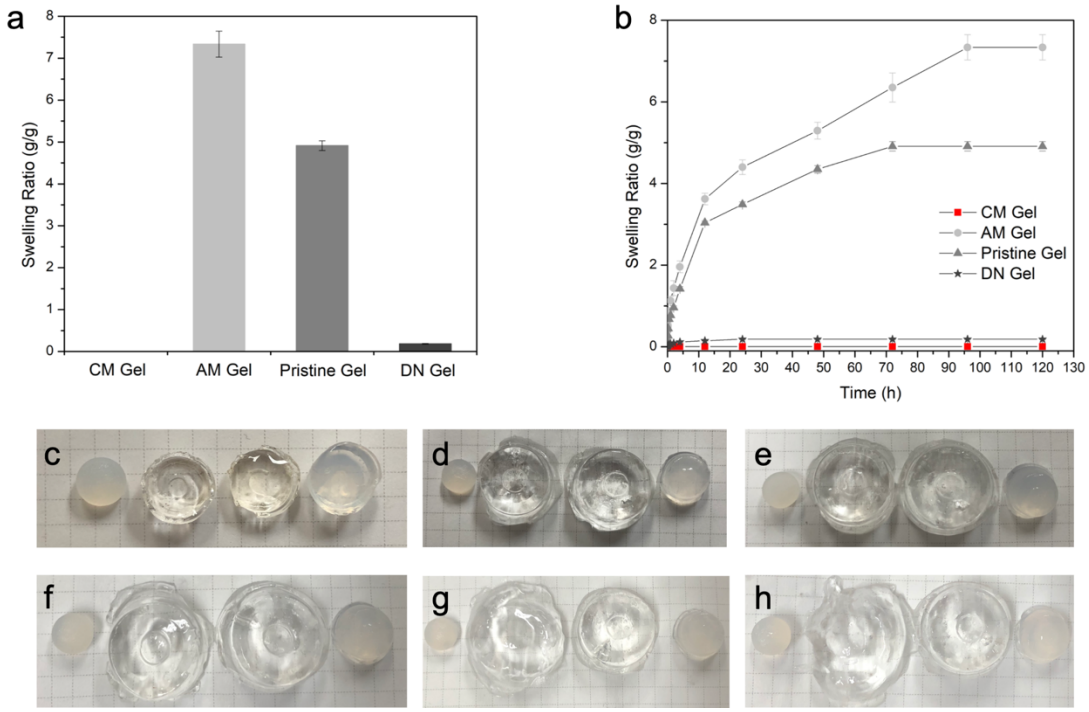

Figure 9 Swelling ratio results. a) Column graph of swelling ratio of different hydrogels at swelling equilibrium stage (n=3). b) Swelling ratio of different hydrogels after predetermined time points(n=3). Photographic images of volume changes of (from left to right) CM, AM, pristine and DN gels after being incubated in DI water for c) 0h, d) 4h, e) 12h, f) 48h, g) 72h and h) 120h.

It is well established that hydrogels' microstructures have vital impacts on their macro-behaviors. That is to say, a more compact microstructure can result in hydrogels with higher stiffness and the smaller pore sizes in a tighter structure can work more effectively on dispersing stress which is also called a load-bearing structure. From the results of SEM images (Figure 10), it was observed that all hydrogels exhibited typical honeycomb-like porous structures which were caused by the evaporation of water. The microstructures of DN hydrogels became much denser than those of the other groups, and the pore sizes sharply decreased to approximately 1μm from 40μm for CM gels, 60μm for AM gels and 20μm for pristine gels, respectively. Notably, the microstructures of DN hydrogels after treating with base for 15min became similar to that of the pristine ones. This variation in microstructures proved the construction and elimination of the CM network.

In summary, taken the confirmation of protonation and deprotonation of CM molecules, the low swelling equilibrium ratio, and the significant differences between DN hydrogels and pristine hydrogels (a reduction of pore sizes of ≈96%) in consideration, it was safe to say that the CM network could be generated based on the mechanism of hydrogen bonds and hydrophobic interactions, and it could be eliminated once the -COOH groups were deprotonated by external chemicals (the base).

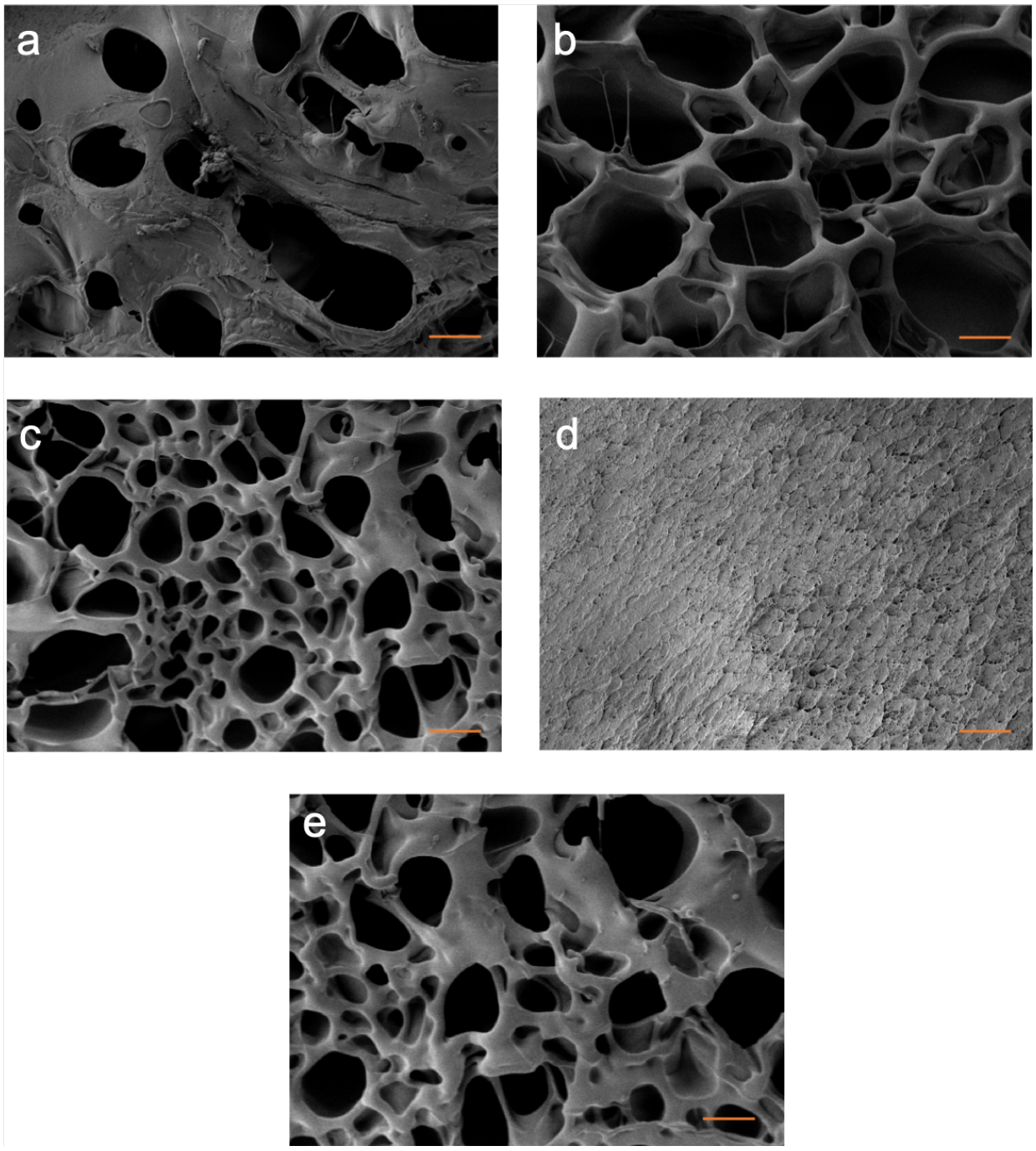

Figure 10 SEM images of a) CM gels, b) AM gels, c) pristine gels, d) DN gels and e) DN gels after basic treatments for 15min. Scale bars = 30μm.

To study the stability of the DN hydrogels, dynamic mechanical properties were measured by oscillatory frequency sweep tests ranging from 0.1 to 100 rad s^{-1} at a fixed deformation strain of 0.01 under room temperature (Figure 11). As expected, G' were steadily higher than G'' in all groups, and both of them were relatively constant during angular changes, indicating stable gel-like properties of all hydrogels in different groups. The G' of DN hydrogels was significantly higher than that of the pristine hydrogels, and it was comparable to that of CM hydrogels. This confirmed the two networks of the DN hydrogels (the PAM network and CM network), and suggested that the generation of the CM network could reinforce hydrogel's stiffness due to denser cross-linking and the rigid nature of this network. Notably, the elevation of G' of pristine and DN hydrogels could be ascribed to the non-covalent bonds, whereas the relative flat traces of CM hydrogels indicated the inflexible polymer CM chains which might be an explanation for the rigidity of the CM network[145-147].

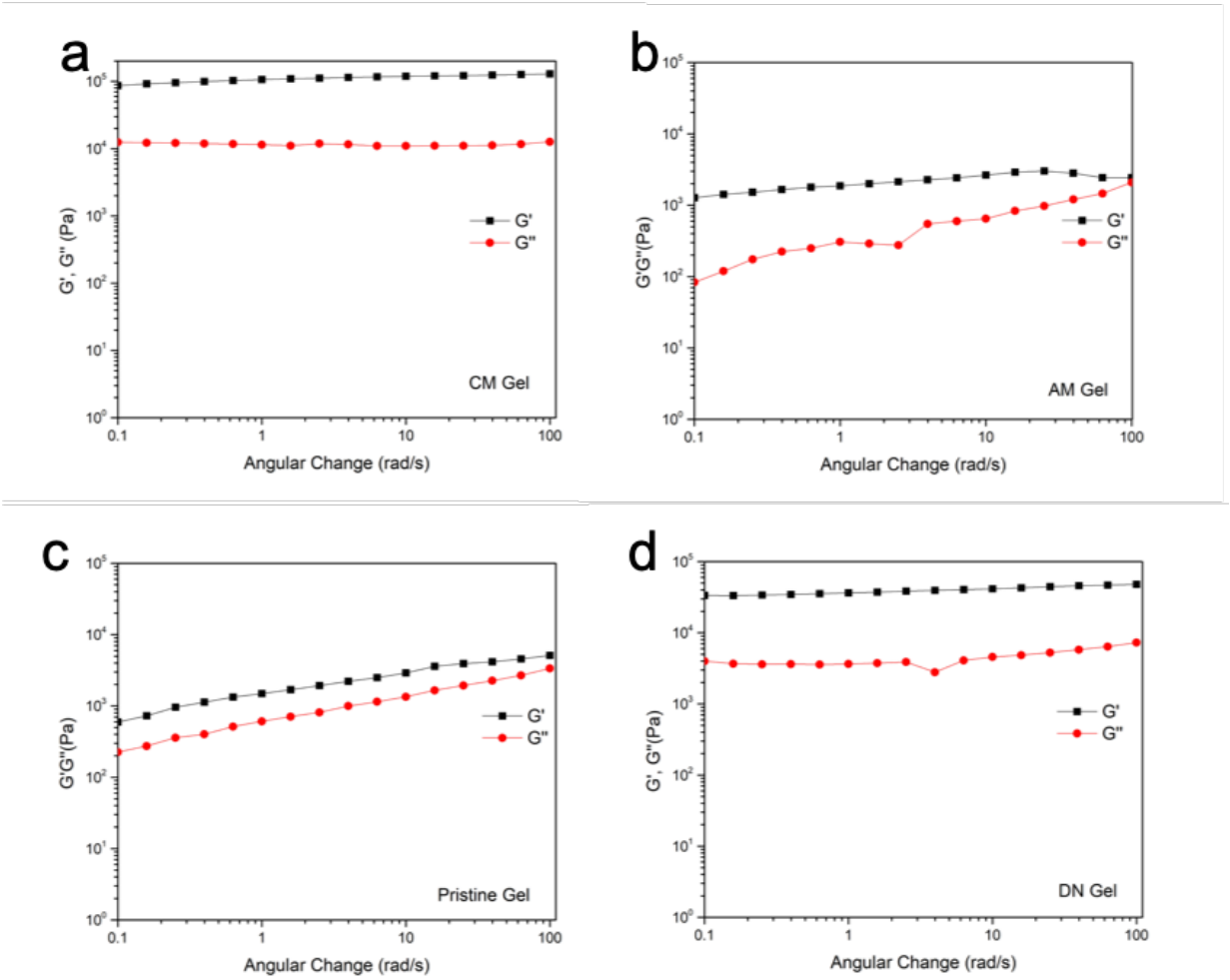

Figure 11 Frequency sweep results of CM, AM, pristine and DN hydrogels showed the good stability of the DN hydrogel during the angular changes of 0.1-100 rad s^{-1} (1% strain).

4.3 Multifunctionality Tests

4.3.1 Reversible Stiffness Changes Behavior

Macroscopic tests were firstly conducted to show the feasibility of reversible stiffness changes. As shown in Figure 12, two ends of the pristine hydrogel strips dropped and stuck side-by-side (Figure 12a) suggesting that hydrogels at this stage (Pristine stage) were soft. Then after incubating in acidic solution for 1min, the DN-1-5% hydrogel strips became "cantilever beam" like whose stiffness were significantly higher than that of the pristine hydrogels and could withstand their own weights (Figure 12b), hydrogels after acidic treatments were considered at "Protonated stage (P stage)". Interestingly, after treating with basic solutions to hydrogels at the P stage, the strips became soft again and showed the same behavior as hydrogels at the Pristine stage (Figure 12c), this stage was defined as "Deprotonated stage (D stage)".

Later on, tensile and compressive tests were carried out to evaluate the stiffness changing abilities quantitatively (Figure 12d-i). Tremendous elastic and tensile modulus increase were observed when comparing DN hydrogels with pristine hydrogels. The tensile elastic modulus was 0.17 MPa for the DN hydrogel which was more than 11 times higher than that of pristine hydrogels (0.015 MPa), and the compressive modulus for DN hydrogels and pristine hydrogels were 1.1 MPa and 0.01 MPa, respectively. The improvements of mechanical strengths were also considerable: compressive stress for DN hydrogels was 3.1 MPa which was approximately 10 times higher than that of the pristine hydrogels (0.38 MPa), and the tensile strength of DN hydrogels dramatically increased from 0.016 MPa of pristine hydrogels to 0.34 MPa of DN hydrogels.

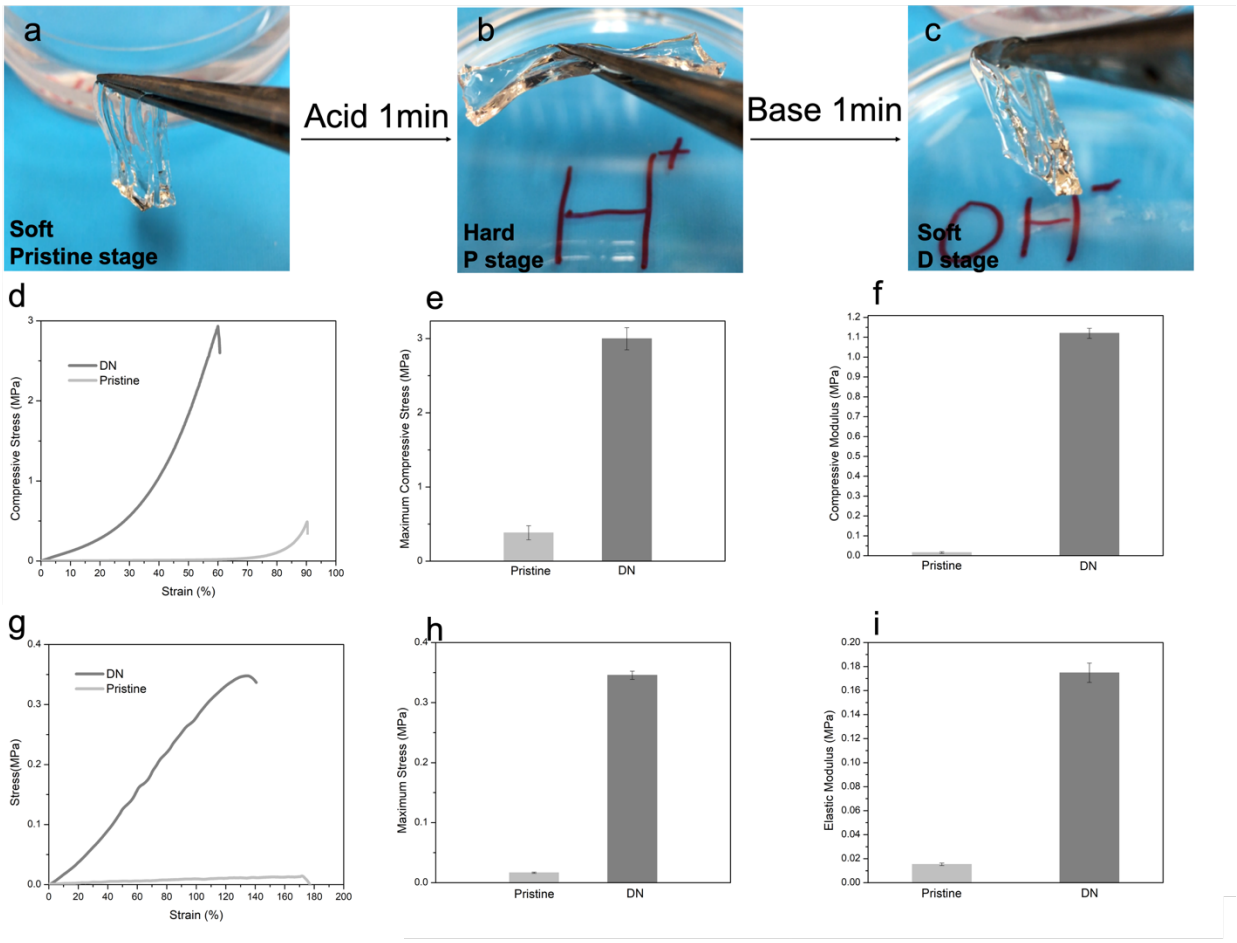

Figure 12 a) Pristine hydrogel strip was soft. b) Hydrogel at the P stage after acidic treatments (0.1M HCl) for 1min became stiff enough to withstand its own weight. c) After basic treatments (0.3M NaOH) for another 1min, hydrogel trip transited to the D stage and regained its softness. d) Compressive curves of DN and pristine hydrogels. e) The maximum compressive stress of DN and pristine hydrogels. f) Compressive modulus of DN and pristine hydrogels. g) Tensile curves of DN and pristine hydrogels. h)The maximum stress of DN and pristine hydrogels. i) Tensile elastic modulus of DN and pristine hydrogels. (n=3)

These improvements of modulus and strength were the results of denser cross-linking after the generation of the CM network. Other than these remarkable mechanical performances of DN hydrogels, one distinctive advantage of this system was that the stiffness could be tuned by simply adjusting the initial CM concentrations or stimuli conditions (i.e., post-crosslinking time and acid concentration).

A more compact microstructure could significantly improve hydrogels' mechanical performances, as the post-crosslinking (acidic treatment) time and the initial CM concentration increased the cross-linking density of hydrogels increased, resulting in gradual changing microstructures from loose to compact (Figure 13). The pore sizes in the microstructures of hydrogels varied from approximately 15μm for DN-30-1% hydrogels and 25μm for DN-1-5% hydrogels to 1μm for DN-30-5% hydrogels. When hydrogels had more compact microstructures, they tended to show improved stiffness. Compressive tests were conducted on DN hydrogels under various post-crosslinking times and initial CM concentrations to show their influence on stiffness changes quantitatively. As shown in Figure 14a-b, the compressive modulus were 0.1 MPa, 0.2 MPa, 0.4 MPa and 1.1 MPa for DN-1-5%, DN-5-5%, DN-15-5% and DN-30-5%, respectively. And the compressive strengths had also increased from approximately 1.25MPa for DN-1-5% hydrogels to almost 3.0 MPa for DN-30-5% hydrogels. The same phenomenon was also observed when increasing the initial CM concentrations. Figure 14c-d show the results for DN-30-1%, DN-30-3% and DN-30-5% hydrogels. The compressive modulus for them were 0.1 MPa, 0.3MPa and 1.1 MPa, respectively. Despite the enhanced modulus and strength, the ductility reduced as the increase of initial CM concentration and post-crosslinking time. The fracture strain for DN-30-5% was 64%, whereas it was 81% for DN-1-5% and 84% for DN-30-1% hydrogels (Figure 14g). This

phenomenon might be the outcome of the incorporated CM network which had an inherent nature of rigidity[148].

The influences of the acidic concentration were also investigated. It was seen from Figure14 e-f that the acidic concentration didn't impact on the maximum stiffness changes, while acids with a higher concentration accelerated the speed of stiffening (i.e., hydrogels reached the maximum stiffness after 15min under 0.3M HCl treatment while it took 30min for 0.1M HCl). Both acidic solutions could reach a stiffness plateau, and the reason for its appearance was believed to be that the CM molecules were fully neutralized after specific incubation times at acidic solutions, and no further property changes shall occur after the ultimate generation of the CM network. An interesting phenomenon was observed during acidic treatments: as the post-crosslinking time increased, the transparency of hydrogels reduced until an optical plateau was reached (Figure 15). And the starting points of the optical plateaus corresponded to that of the stiffness plateaus. This showed a possibility to develop a more straightforward and efficient way to determine the process of micro-reactions by macro-phenomena.

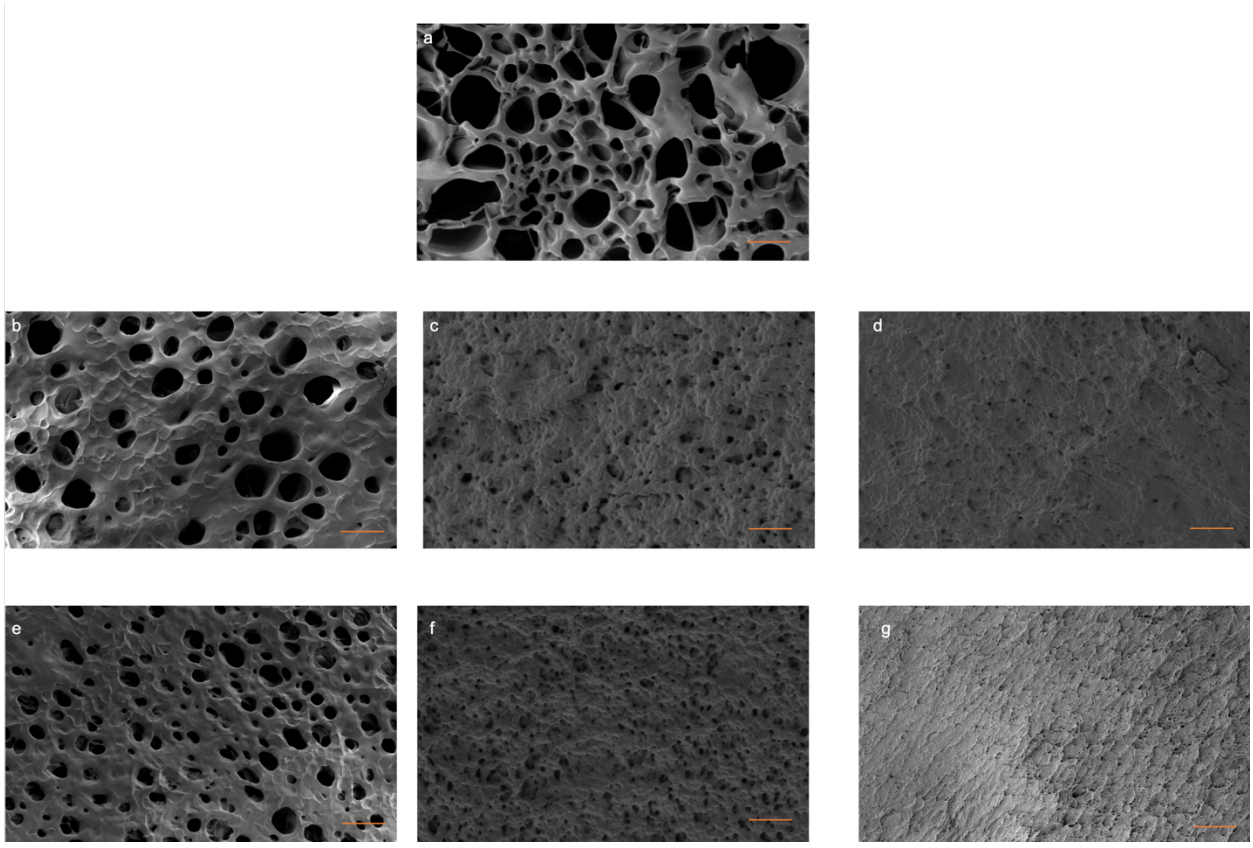

Figure 13 SEM images of a) pristine hydrogels, b) DN-1-5% hydrogels, c) DN-5-5% hydrogels, d) DN-15-5% hydrogels, e) DN-30-1% hydrogels, f) DN-30-3% hydrogels and g) DN-30-5% hydrogels. Scale bars = 30µm.

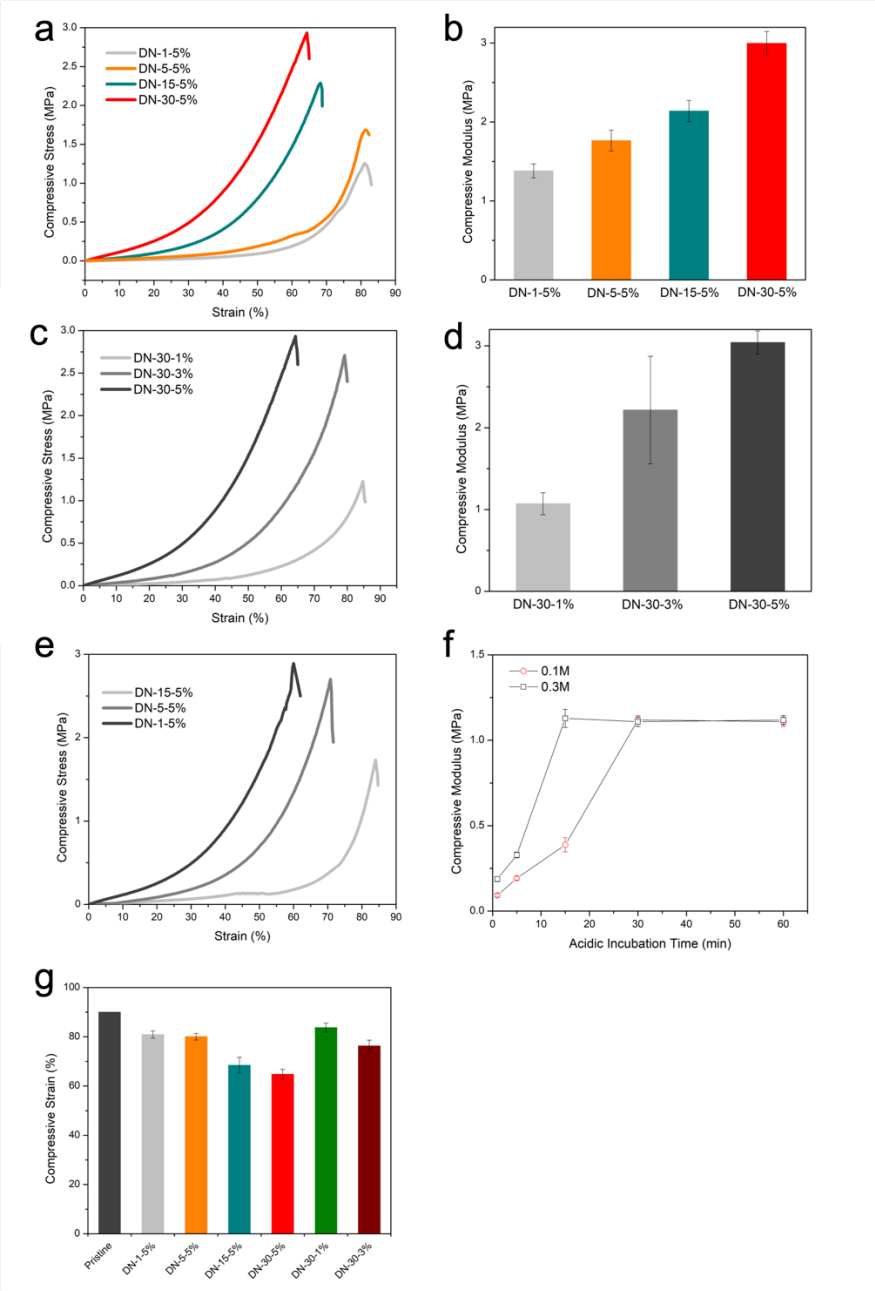

Figure 14 a) Compressive curves of DN-x-5% hydrogels, where x=1, 5, 15, 30. b) Compressive modulus of DN-x-5% hydrogels, where x=1, 5, 15, 30. c) Compressive curves of DN-30-y hydrogels, where y=1, 3, 5. d) Compressive modulus of DN-30-y hydrogels, where y=1, 3, 5. e) Compressive curves of DN-x-5% hydrogels, where x=1, 5, 15, and the acid used here to induce CM network was 0.3M HCl. f) Compressive modulus changed as acidic incubation time increased, and a higher acidic concentration accelerated the speed to achieve the maximum stiffness change. g) Compressive strain at break for different hydrogels. (n=3)

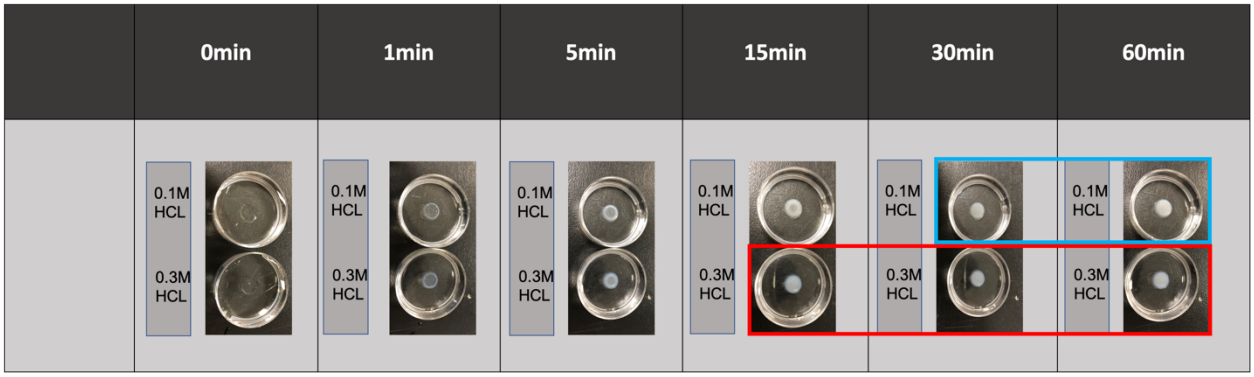

Figure 15 Optical changes of DN hydrogels under the treatments of different acidic solutions at predetermined time points.

As shown in the macroscopic tests, the DN hydrogel system was able to perform reversible stiffness changes. And the compressive tests showed that the stiffness increased greatly from 0.01 MPa to 0.1 MPa after incubation in acid for 1min. Therefore, the fast-reversible stiffness changes were evaluated by cyclic acid-base treatments on hydrogels. Hydrogels were transited between P stages and D stages repeatedly, P_n/D_n represented the stages where hydrogels were at after specific treatments (acid/base), for example, P_1 represented the stage after applying the first acidic treatment to pristine hydrogels, D_1 represented the stage after applying first basic treatment to P_1 hydrogels. As shown in Figure 16a-d, three consecutive acid-base treatments were applied to cylindrical hydrogels and compressive tests were conducted to show the reversible stiffness changes. Hydrogels at P_n stages had 0.1 MPa of compressive modulus and hydrogels at D_n stages had 0.01 MPa of compressive modulus, suggesting good stiffness reversibility. This property was also subjected to rheological profiles (Figure 16e). A stable solid hydrogel was maintained during the whole treatments (G' > G''), and the change of G' after acidic and basic treatments proved the reversible stiffness.

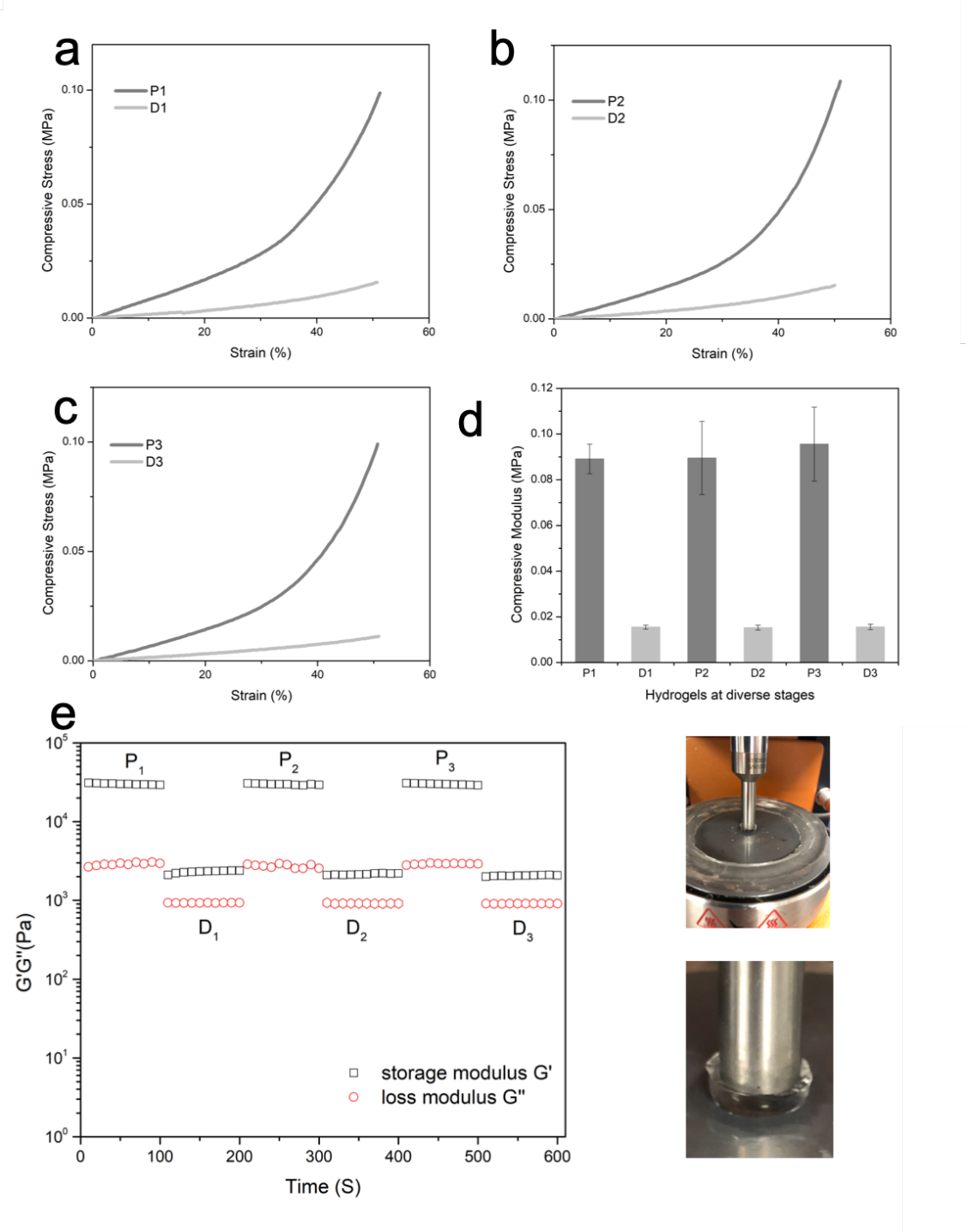

Figure 16 a-c) Compressive curves of the first/second/third acid-base cyclic tests. d) Compressive stress of hydrogels at diverse stages (n=3). e) G' and G'' as a function of hydrogels at different stages. Each treatment lasted for 1min.

4.3.2 Self-Healing Performance

The reversible generation and elimination of the second network (CM network) of this DN hydrogel system gave rise to the stimuli-responsive self-healing performance. Macroscopic experiments were performed at first. As shown in Figure 17a-d, the cut hydrogel strips and broken "hearts" were healed after acidic treatments, and after putting the healed ones in DI water for 3h, they could remain integrity indicating that sufficient physical interactions by the generation of the CM network instead of simple adhesion took place at the interfaces. Then after basic treatments, the "heart" broke into halves, and the wedge cut reappeared on the hydrogel strips. This self-healing could be repeatedly performed without hysteresis.

The underlying mechanism for such self-healing behavior could be interpreted as follow: the CM chains inside hydrogels diffused more fluently and freely at Pristine/D stages, therefore, the CM chains diffused across fracture/contacted sites, and the acidic solutions worked as the "catalyzer" which was mentioned in the biomimetic approaching via the "bleeding" mechanism to trigger the formation of the CM network therefore healing the wounded parts. Rheology tests have further demonstrated this property. As illustrated in Figure 17e-f, there were no cross points on G' and G'' traces from low strain (1%) to high strain (700%) of pristine hydrogels, this suggested that the pristine hydrogels possessed non-autonomous self-healing ability, and the sudden drops of G' and G'' were ascribed to the collapse of hydrogel networks. The liquid-like property after basic treatments of CM molecules enabled the diffusion at Pristine/D stages, whereas its gel-like property after acidic treatments enabled the ability to self-heal. These results had confirmed that this self-healing behavior was due to the generation and elimination of the CM network.

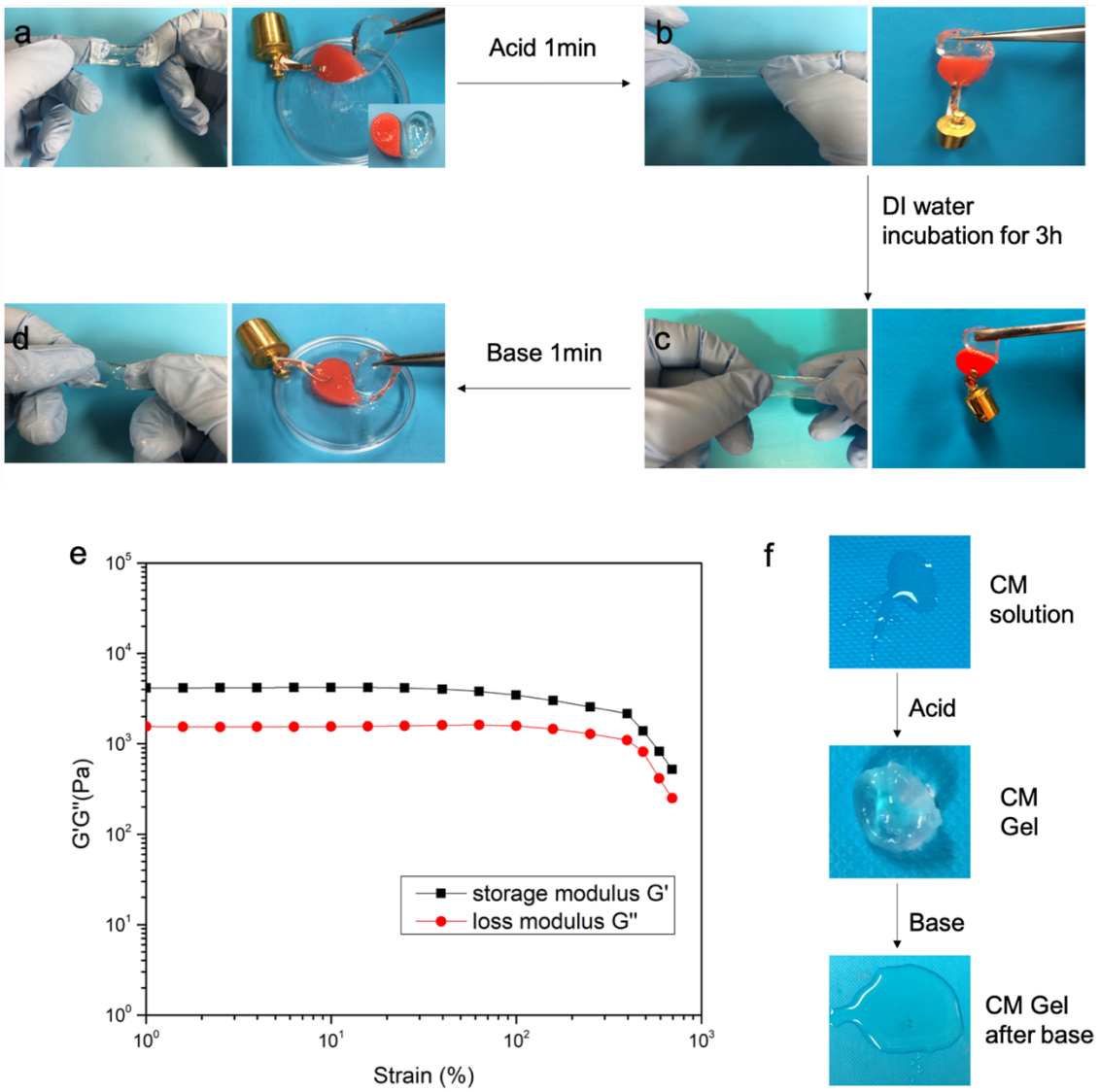

Figure 17 Macroscopic self-healing tests: a) before acid the hydrogel strip had a wedge and "heart" was broke into halves, b) after acidic treatment, both of them healed, c) then they were placed in DI water for 3h and remained integration showing that the healing was caused by physical interactions (CM network) rather than simple adhesion, d) while after basic treatment, the wedge reappeared and the "heart" again separated into halves. e) The results of G' and G'' of the pristine hydrogels at strain amplitude sweep tests ranging from 1% to 700% at a fixed angular frequency at 10 rad s^{-1}. f) The sol-gel transformation of CM gel in the presence of external stimuli proved that the self-healing was a result of the formation/elimination of the CM network.

To quantitatively measure the self-healing property, self-healing efficiency (SE) was introduced. SE is defined as the ratio of healing strength at break of SE-*x*-*y* hydrogels ($Break_{SE\text{-}x\text{-}y}$) versus the strength of corresponded DN-*x*-*y* hydrogels ($Break_{DN\text{-}x\text{-}y}$), where SE stands for self-healed, *x* and *y* have the same meaning as they are in DN-*x*-*y*, it is calculated as $SE = (Break_{healed}/Break_{DN\text{-}x\text{-}y}) * 100\%$ [24]. Firstly, the maximum tensile strengths of DN-*x*-1%, DN-*x*-3% and DN-*x*-5% hydrogels were determined, and experiments indicated that all of them could reach their maximum strength when $x = 30$ (Figure 18). Self-healing experiments were conducted on hydrogel strips (Figure 19a) via tensile tests. The concentrations of acidic solutions had no impact on the maximum SE while a higher concentration favored the self-healing speed, which showed the same behavior as that of stiffness changes (Figure 19b). The halves could rapidly self-heal within 1min possessing a SE of 23%, and the SE increased as the healing time elongated to 47% for SE-5-5%, 69% for SE-15-5% and a maximum 91% for SE-30-5% (Figure 19c-d). However, unlike the CM-concentration-dependent behavior in stiffness changes, the initial CM concentration had no significant influence on the SE (i.e., 82%, 74% and 91% for SE-30-1%, SE-30-3% and SE-30-5%, respectively) (Figure 19e-f). In summary, this DN hydrogel system exhibited reversible and high-efficient self-healing properties.

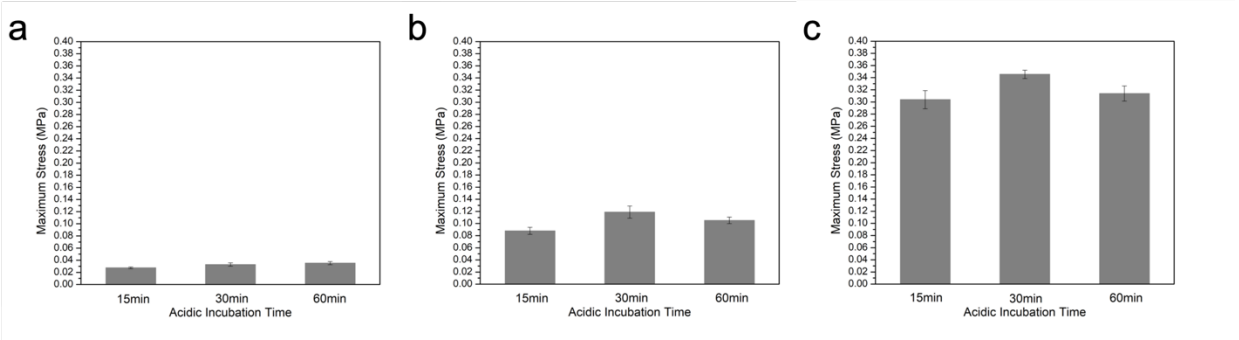

Figure 18 Tensile strengths of a) DN-x-1%, b) DN-x-3% and c) DN-x-5% hydrogels, where x = 15, 30 and 60. (n=3)

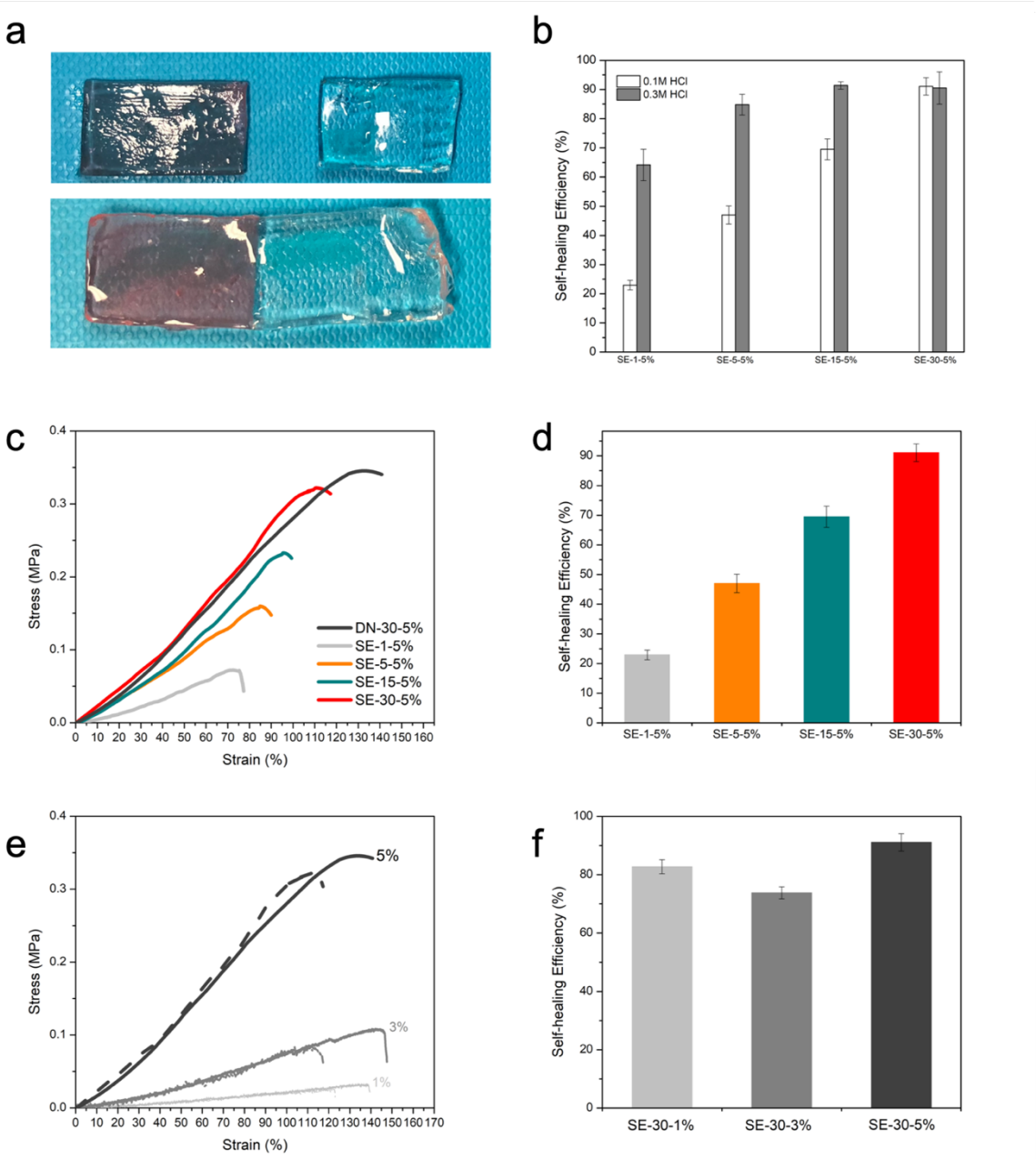

Figure 19 a) Self-healing tests were conducted on this end-to-end model. b) Self-healing efficiency of DN hydrogels under different acidic solutions (0.1/0.3M HCL). c-d) The SE of DN hydrogels increased under prolonged acidic treatments. e-f) The SE of DN hydrogels with different initial CM concentrations, in here, the SE was compared between the tensile stress of healed ones (dotted lines) and the tensile stress of the un-cut ones (solid lines) with the same CM concentrations, i.e., the healed SE-1% compared to the uncut DN-1%. (n-3)

4.3.3 Shape-memory Ability

On the basis of reversible and significant stiffness transitions within a short time and the good resilience in Pristine/D stages, the DN hydrogel system was expected to possess excellent shape-memory abilities. Figure 20 gave a few examples of the shape-memory models. The V, strip and square models were twisted, elongated and expanded to temporary shapes which were immediately fixed after incubation in acidic solutions for 30s, then they recovered to original shapes after incubating in basic solutions within 60s. Based on the complexity of deformation, the incubation time required for full recoveries might vary a little.

To determine the shape-memory abilities, shape-fixing efficiency (F) and shape-recovery ratio (RR) were introduced. F represents hydrogels' ability to hold their fixed shapes and RR stands for the ability to go back to the initial shapes, calculation for those are as follows: $F=(\ell_a-\ell_v)/(\ell_f-\ell_v)$, $R=(\ell_f-\ell_b)/(\ell_f-\ell_v)$, where ℓ_v, ℓ_a, and ℓ_f are lengths of virgin samples, fixed stretched samples (hydrogels at P_n stages) and samples after resting the fixed stretched ones under different environment for a certain amount of time, and ℓ_b represents the lengths of the hydrogel strips after basic treatments (hydrogels at D_n stages)[23]. The lengths of the hydrogel strips were measured to calculate F and RR, and the results were shown in Figure 21. F for hydrogels at P_n stages was relatively the same regardless of the testing environment (i.e., 99% ± 0.01% for DI water ones and 100% ± 0 for hermetical ones) (Figure 21a). The lengths, widths, thicknesses and weights of hydrogels at fixed shapes were measured after placing them in hermetical containers for 3h, and all of the parameters were approximately the same indicating the stable shape-fixing ability of this system (Figure 21b).

The RR was 97% ± 1.8% after three consecutive deforming – fixing – recovery circles (Figure 21c-d). Thus, this hydrogel could attain ≈100% shape-fixing efficiency and shape-recovery ratio within 1min, which ranks one of the best among current developed shape-memory hydrogels.

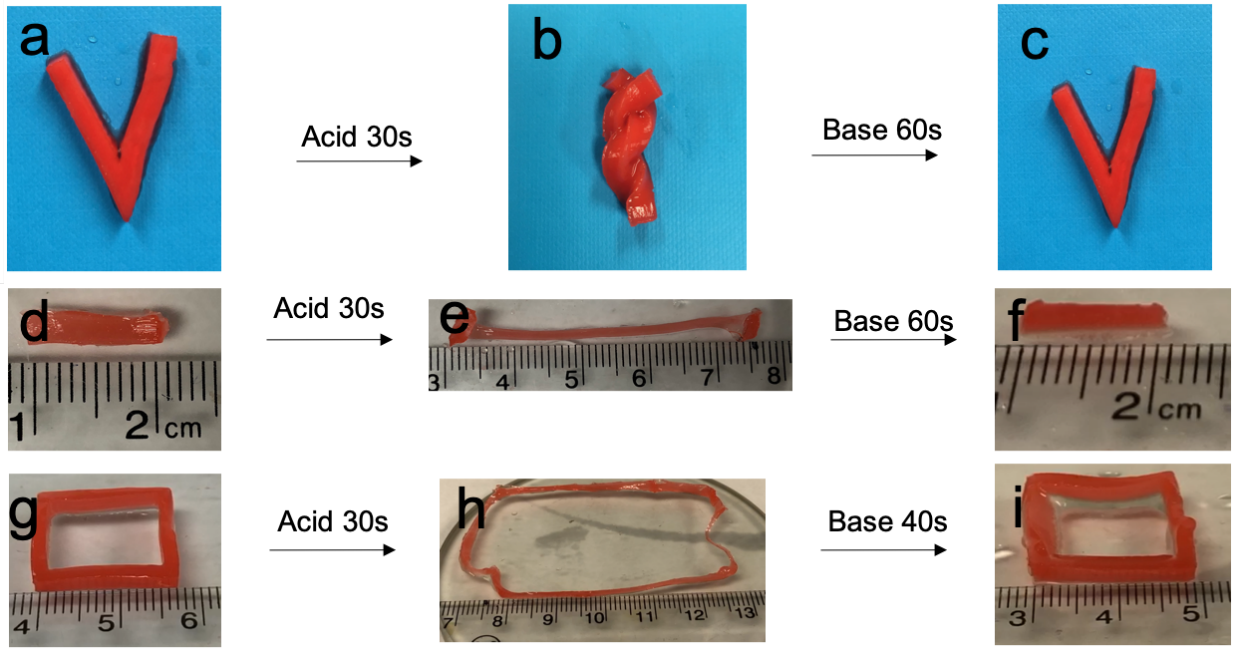

Figure 20 Fast shape-memory behaviors of the CM-based DN hydrogel. a-c) Twisted model. d-f) Elongation model.)g-i Expanded model.

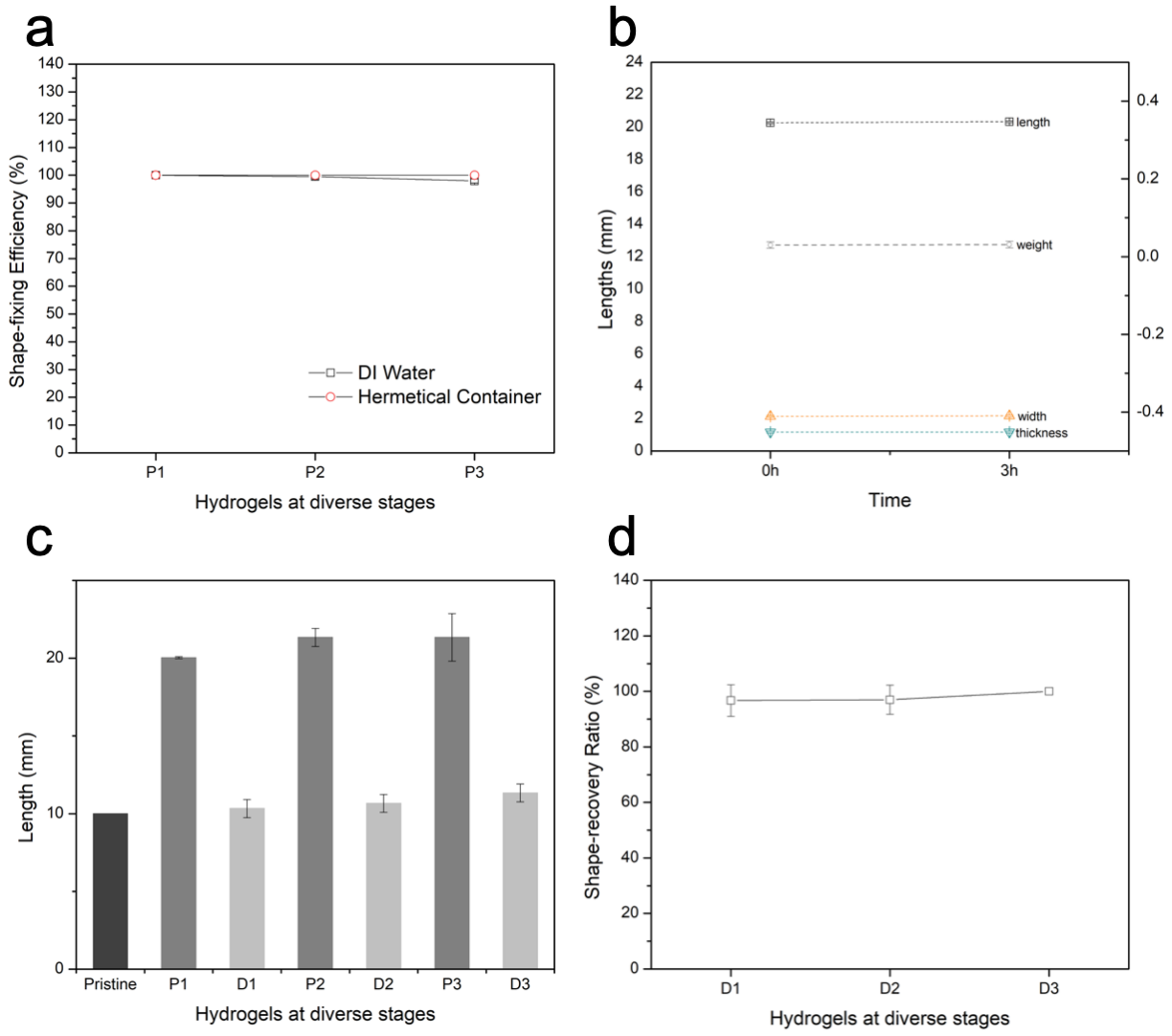

Figure 21 a) Shape-fixing efficiency profile of hydrogels at $P_{1/2/3}$ stages, black hollow squares represent fixity measurement conducted to hydrogels placed in DI water while red hollow circles represent fixity results of hydrogels placed in hermetical containers. b) Length, width, thickness and weight changes for P_1 hydrogels after being placed in hermetical containers for 3 hours. c) Hydrogel strip samples' lengths at different stages. d) Shape-recovery ratio of hydrogels at $D_{1/2/3}$ status. (n=3)

4.4 Potential Applications

4.4.1 Motion Sensor and "On-demand" Switch

Carbon nanotubes are wildly used to bestow good conductivity to hydrogels without impairing other properties[149]. We incorporated CNTs in pristine hydrogels, and it could be seen from Figure 22a that the resistance of hydrogels reduced as the prolonged acidic treatment time showing an improved conductivity. This resistance reduction might be because the generation of the CM network induced a denser cross-linking structure which created a more uniform dispersion of CNTs. CNTs-incorporated hydrogels are well-studied for their motion sensing abilities upon mechanical stimuli. Cuboid hydrogels were attached to the index finger to act as a bio-sensor (Figure 22b), and normalized resistance ($R-R_0/R_0$, where R was the resistance when the index finger was straightly placed and R_0 was the resistance when the index finger curved) was plotting in Figure 22c-d. The resistance was recorded to simultaneously wave with the reciprocation of the index finger at both low speed and high speed. The possible reason for this kind of resistance variation was that during the finger movement, the thickness of hydrogels decreased creating a better interconnection and alignment of CNTs [150, 151]. This showed that the as-designed hydrogel system can be utilized as bio-sensor with good sensitivity.

Another potential application is the "on-demand" switch in electrical circuits. As shown in Figure 22e-f, the hydrogel strip was firstly curved and fixed by acid and placed in an open circuit with the LED bulb off, after applying base on the surface of the curvature, the hydrogel recovered to its original shape (flat) therefore switching-on the circuit and illuminating the LED bulb.

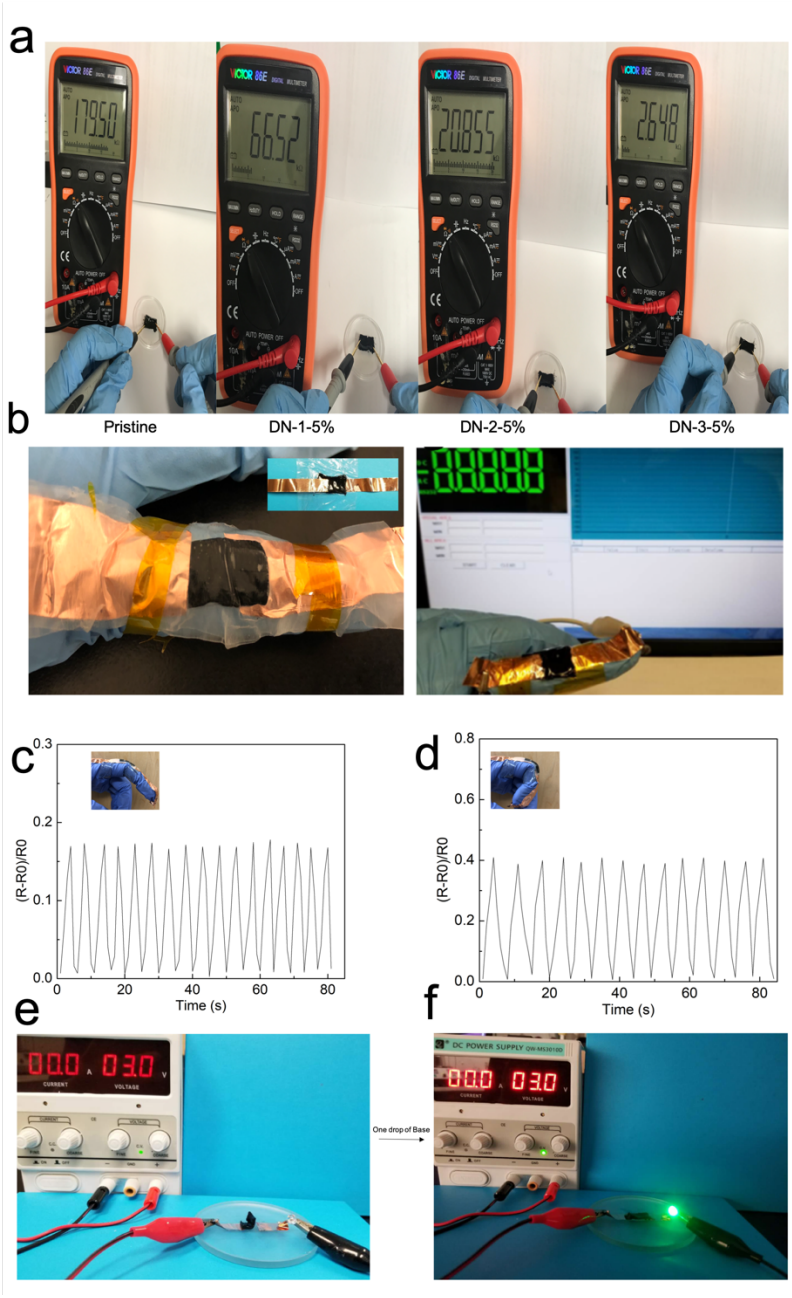

Figure 22 a) The resistances of pristine, DN-1-5%, DN-2-5% and DN-3-5% hydrogels. b) Illustration of the motion sensor device. Hydrogel works as a motion sensor, the relative resistance defined as $(R-R_0)/R_0$ as a function of time were introduced to measure the sensitivity, results of c) 45˚ bend and d) 90˚ bend. e-f) One flat hydrogel strip was fixed into a temporary shape with a curvature of 90˚using 0.1M HCl, it was then attached to one cupper strip in a circuit where another cupper strip was distantly placed beside.

4.4.2 “LEGO-Like” 3D Printing Ink

Three-dimensional (3D) printing has attracted many attentions in recent years due to its paramount importance in the fabrications of scaffolds, cell culture, etc[152, 153]. However, the difficulty to print sophisticated objectives is one sound barrier of 3D printing applications. Thus, here we proposed a “LEGO-like” 3D printing ink by using the CM-based DN hydrogel system. Since the viscosity increased as the increase of CM concentrations in the precursor solutions, and precursor solutions contained 18% w/v of CM were found to be ideal for 3D printing after pre-testing. The “LEGO-like” printing via this CM-based ink was performed in three steps: printing – gelation – assembling. As shown in Figure 23a-d, two meshes were printed first, and then they were gelled to stable pristine hydrogel meshes after TEMED treatments through the gelation of the PAM network, finally, the meshes were assembled into desired shapes after attaching certain parts together and being incubated into acid for 60s. Figure 23e-j show the 3D printing demonstrations of more complex objectives: they were firstly divided into simple parts like circles, squares, etc., then the parts were printed separately and gelled, and finally, these parts were assembled by healing specific parts together through acidic treatments to get the desired shapes.

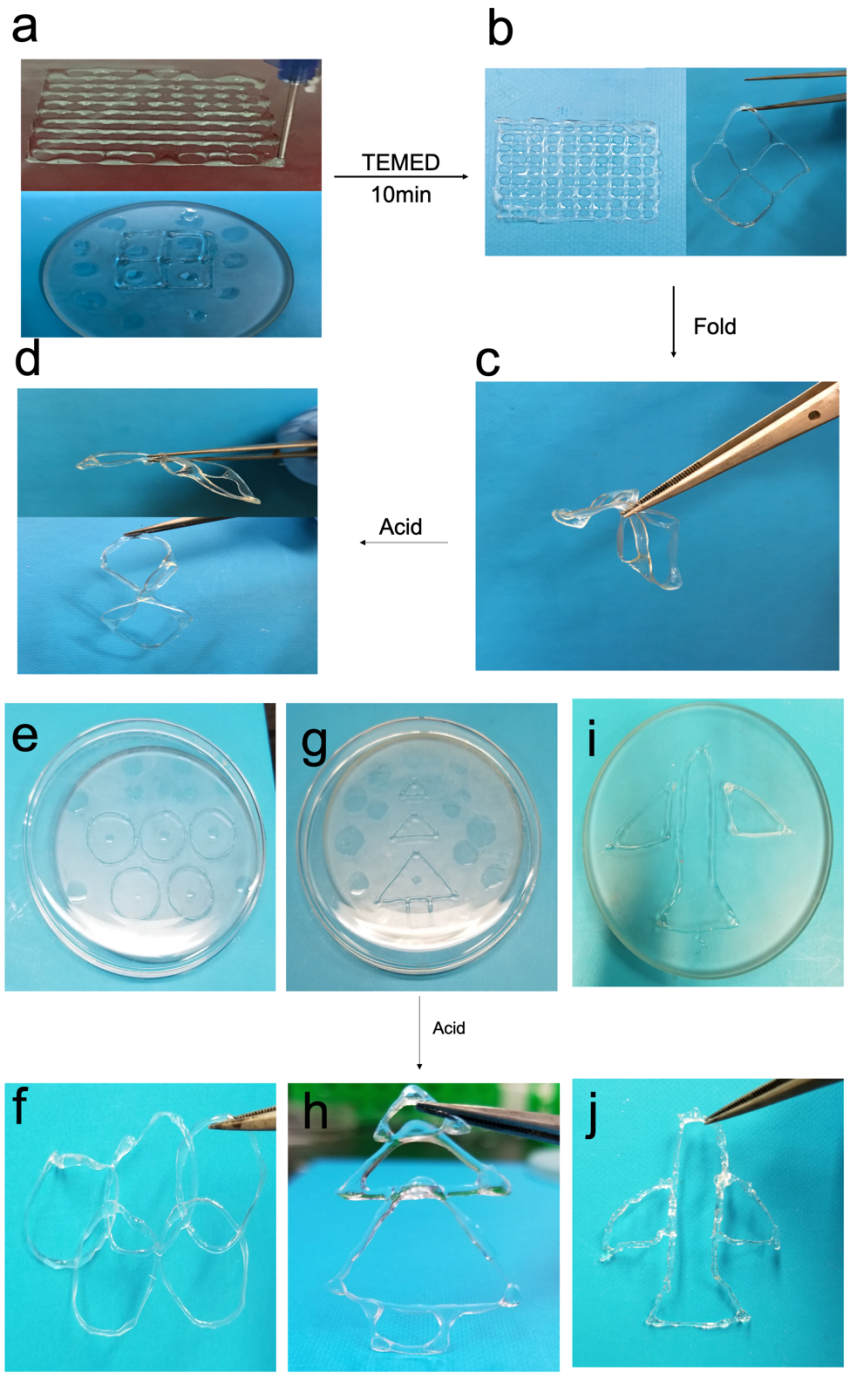

Figure 23 a-d) Illustration of three-step 3D printing. Examples of "LEGO" property, e,f)Olympic rings, g-h) Christmas trees, i-j) airplanes.

Chapter 5

Summary and Conclusions

The major findings and discoveries are summarized as follows,

1. This is the first study reporting the gelation of CM, and using it as the key factor to build a DN hydrogel system that has multiple features.
2. The CM-based DN hydrogels can perform reversible stiffness changes which is considered as a rare ability to most of the hydrogels, and it provides a new set of combination for DN constructions with such properties. And the stiffness changes of CM-based DN hydrogels are comparable to most of the currently developed hydrogels. Considering the unique biocompatibility and biodegradation properties of CM, this DN hydrogel system can be applied in biomedical areas such as drug delivery, scaffolds, wound dressings, etc.
3. The reversible CM network can be used through the "bleeding" mechanism to endow hydrogels with self-healing abilities. It is tested to show a rapid self-healing behavior within 1min with a 23% self-healing efficiency, and it has up to 91% self-healing efficiency within 30min. Furthermore, it is believed that the self-healing speed can be improved by tuning stimuli conditions.
4. The CM-based DN hydrogel system possesses excellent shape-memory abilities (~100% of shape-fixing efficiency and shape-recovery ratio). The ideal F and RR indicate its potential to be used as shape-memory materials.

5. The CNTs-incorporated hydrogels exhibited different resistances after different acidic treatment times. And it can also be used as the “on-demand” switch when combining with its shape-memory abilities. Therefore, this hydrogel can be used as pH indicators, acid sensors or “on-demand” switches triggered by pH changes. And it is proven to have high sensitivity when using as the biosensor to detect real-time moving.
6. The CM-based DN hydrogel opens the door to simplify 3D printing for sophisticated objectives by combining its 3D printability and self-healing properties.
7. Overall, this is the first CM-based multifunctional DN hydrogel system that has great potential in biomedical uses.

Chapter 6

Suggestions for Future Work

1. In order to have a full understanding of the influence factors of the properties, CMs with different substitution degrees and deacetylation degrees are suggested to be further studied.
2. Different CM-based DN system should be investigated in future studies to assess the versatility.
3. Since the CM has good biological properties, *in vivo* tests should be applied to broaden its biomedical uses.

References

1. Khor, E. and L.Y.J.B. Lim, *Implantable applications of chitin and chitosan.* Biomaterials, 2003. **24**(13): p. 2339-2349.
2. Suh, J.K. and H.W. Matthew, *Application of chitosan-based polysaccharide biomaterials in cartilage tissue engineering: a review.* Biomaterials, 2000. **21**(24): p. 2589-98.
3. Drury, J.L. and D.J. Mooney, *Hydrogels for tissue engineering: scaffold design variables and applications.* Biomaterials, 2003. **24**(24): p. 4337-51.
4. Yuk, H., et al., *Hydraulic hydrogel actuators and robots optically and sonically camouflaged in water.* Nature, 2017. **8**: p. 14230.
5. Jiang, W., et al., *Photoresponsive soft‐robotic platform: biomimetic fabrication and remote actuation.* Advanced Functional Materials, 2014. **24**(48): p. 7598-7604.
6. Tai, Y., et al., *A highly sensitive, low-cost, wearable pressure sensor based on conductive hydrogel spheres.* Nanoscale, 2015. **7**(35): p. 14766-73.
7. Gao, W., et al., *Fully integrated wearable sensor arrays for multiplexed in situ perspiration analysis.* 2016. **529**(7587): p. 509.
8. Montero de Espinosa, L., et al., *Bioinspired polymer systems with stimuli-responsive mechanical properties.* Chemical Reviews, 2017. **117**(20): p. 12851-12892.
9. Guvendiren, M. and J.A. Burdick, *Stiffening hydrogels to probe short- and long-term cellular responses to dynamic mechanics.* Nat Commun, 2012. **3**: p. 792.
10. Leipzig, N.D. and M.S. Shoichet, *The effect of substrate stiffness on adult neural stem cell behavior.* Biomaterials, 2009. **30**(36): p. 6867-78.
11. Huang, W.M., et al., *Shaping tissue with shape memory materials.* Adv Drug Deliv Rev, 2013. **65**(4): p. 515-35.
12. Qiu, Y. and K. Park, *Environment-sensitive hydrogels for drug delivery.* Adv Drug Deliv Rev, 2001. **53**(3): p. 321-39.
13. Guo, W., et al., *pH-stimulated DNA hydrogels exhibiting shape-memory properties.* Adv Mater, 2015. **27**(1): p. 73-8.
14. Hu, Y., et al., *A Shape-Memory DNA-Based Hydrogel Exhibiting Two Internal Memories.* Angew Chem Int Ed Engl, 2016. **55**(13): p. 4210-4.
15. Wang, Y., et al., *Synthesis of cellulose-based double-network hydrogels demonstrating high strength, self-healing, and antibacterial properties.* Carbohydr Polym, 2017. **168**: p. 112-120.
16. Sottos, N., S. White, and I. Bond, *Introduction: self-healing polymers and composites.* J R Soc Interface, 2007. **4**(13): p. 347-8.
17. Zhao Wei, J.H.Y., Zhen Qi Liu, Feng Xu, Jin Xiong Zhou, Miklós Zrínyi, Yoshihito Osada, and Yong Mei Chen, *Novel Biocompatible Polysaccharide-Based Self-Healing Hydrogel.* Advanced Functional Materials, 2015. **25**(9): p. 1352-1359.
18. Taylor, D.L. and M. In Het Panhuis, *Self-Healing Hydrogels.* Adv Mater, 2016. **28**(41): p. 9060-9093.
19. Capadona, J.R., et al., *Stimuli-responsive polymer nanocomposites inspired by the sea*

cucumber dermis. Science, 2008. **319**(5868): p. 1370-4.
20. Mendez, J., et al., *Bioinspired mechanically adaptive polymer nanocomposites with water-activated shape-memory effect.* Macromolecules, 2011. **44**(17): p. 6827-6835.
21. Yang, F.K., et al., *A hybrid material that reversibly switches between two stable solid states.* 2019. **18**(8): p. 874.
22. Darabi, M.A., et al., *Skin-Inspired Multifunctional Autonomic-Intrinsic Conductive Self-Healing Hydrogels with Pressure Sensitivity, Stretchability, and 3D Printability.* Adv Mater, 2018. **30**(4).
23. Gulyuz, U. and O.J.M. Okay, *Self-healing poly (acrylic acid) hydrogels with shape memory behavior of high mechanical strength.* Macromolecules, 2014. **47**(19): p. 6889-6899.
24. Wei, Z., et al., *Novel biocompatible polysaccharide - based self - healing hydrogel.* Advanced Functional Materials, 2015. **25**(9): p. 1352-1359.
25. Nakahata, M., et al., *Redox-responsive self-healing materials formed from host-guest polymers.* Nat Commun, 2011. **2**: p. 511.
26. White, S.R., et al., *Autonomic healing of polymer composites.* Nature, 2001. **409**(6822): p. 794-7.
27. Francis Suh, J.K. and H.W.T. Matthew, *Application of chitosan- based polysaccharide biomaterials in cartilage tissue engineering: a review.* Biomaterials, 2000. **21**(24): p. 2589-2598.
28. Croisier, F. and C.J.E.P.J. Jérôme, *Chitosan-based biomaterials for tissue engineering.* European Polymer Journal, 2013. **49**(4): p. 780-792.
29. Suh, J.-K.F. and H.W.J.B. Matthew, *Application of chitosan-based polysaccharide biomaterials in cartilage tissue engineering: a review.* Biomaterials, 2000. **21**(24): p. 2589-2598.
30. Ladet, S., L. David, and A. Domard, *Multi-membrane hydrogels.* Nature, 2008. **452**(7183): p. 76-9.
31. Wang, C., et al., *Shape-memory and self-healing functions of DNA-based carboxymethyl cellulose hydrogels driven by chemical or light triggers.* Chemical science, 2018. **9**(35): p. 7145-7152.
32. Wang, C., et al., *DNA-Based Hydrogels Loaded with Au Nanoparticles or Au Nanorods: Thermoresponsive Plasmonic Matrices for Shape-Memory, Self-Healing, Controlled Release and Mechanical Applications.* ACS nano, 2019.
33. Wang, C., et al., *Stimuli -Responsive Donor–Acceptor and DNA -Crosslinked Hydrogels: Application as Shape - Memory and Self - Healing Materials.* Advanced Functional Materials, 2018. **28**(35): p. 1803111.
34. Zhao, Z., et al., *Biphasic Synergistic Gel Materials with Switchable Mechanics and Self-Healing Capacity.* Angewandte Chemie International Edition, 2017. **56**(43): p. 13464-13469.
35. Xu, D., et al., *High - Flexibility, High - Toughness Double - Cross - Linked Chitin Hydrogels by Sequential Chemical and Physical Cross -Linkings.* Advanced Materials, 2016. **28**(28): p. 5844-5849.
36. Haraguchi, K. and T. Takehisa, *Nanocomposite Hydrogels: A Unique Organic–Inorganic*

Network Structure with Extraordinary Mechanical, Optical, and Swelling/ De - swelling Properties. Advanced Materials, 2002. **14**(16): p. 1120-1124.
37. Liu, Y., et al., *Highly flexible and resilient elastin hybrid cryogels with shape memory, injectability, conductivity, and magnetic responsive properties.* Advanced Materials, 2016. **28**(35): p. 7758-7767.
38. Bilici, C., et al., *Melt-processable shape-memory hydrogels with self-healing ability of high mechanical strength.* Macromolecules, 2016. **49**(19): p. 7442-7449.
39. Tao Lin, S., et al., *Physical hydrogels composed of polyampholytes demonstrate high toughness and viscoelasticity.* Nature Materials, 2013. **12**(10): p. 932.
40. Yang, Y., et al., *A Universal Soaking Strategy to Convert Composite Hydrogels into Extremely Tough and Rapidly Recoverable Double - Network Hydrogels.* Advanced Materials, 2016. **28**(33): p. 7178-7184.
41. Drury, J.L. and D.J. Mooney, *Hydrogels for tissue engineering: scaffold design variables and applications.* Biomaterials, 2003. **24**(24): p. 4337-4351.
42. Hoare, T.R. and D.S.J.P. Kohane, *Hydrogels in drug delivery: Progress and challenges.* Polymer, 2008. **49**(8): p. 1993-2007.
43. Kim, S.W., Y.H. Bae, and T.J.P.r. Okano, *Hydrogels: swelling, drug loading, and release.* pharmaceutical research, 1992. **9**(3): p. 283-290.
44. Lee, K.Y. and D.J.J.C.r. Mooney, *Hydrogels for tissue engineering.* Chemical Reviews, 2001. **101**(7): p. 1869-1880.
45. Russell, R.J., et al., *A fluorescence-based glucose biosensor using concanavalin A and dextran encapsulated in a poly (ethylene glycol) hydrogel.* Analytical chemistry, 1999. **71**(15): p. 3126-3132.
46. Quinn, C.A., R.E. Connor, and A.J.B. Heller, *Biocompatible, glucose-permeable hydrogel for in situ coating of implantable biosensors.* Biomaterials, 1997. **18**(24): p. 1665-1670.
47. Wang, G., et al., *Amperometric hydrogen peroxide biosensor with sol–gel/chitosan network-like film as immobilization matrix.* biosensors and bioelectronics, 2003. **18**(4): p. 335-343.
48. Xue, Z., et al., *A novel superhydrophilic and underwater superoleophobic hydrogel - coated mesh for oil/water separation.* Advanced Materials, 2011. **23**(37): p. 4270-4273.
49. Gao, H., et al., *Mussel-inspired synthesis of polydopamine-functionalized graphene hydrogel as reusable adsorbents for water purification.* ACS applied materials & interfaces, 2013. **5**(2): p. 425-432.
50. Rudzinski, W.E., et al., *Hydrogels as controlled release devices in agriculture.* Designed monomers and polymers, 2002. **5**(1): p. 39-65.
51. Ullah, F., et al., *Classification, processing and application of hydrogels: A review.* Materials Science and Engineering: C., 2015. **57**: p. 414-433.
52. Schexnailder, P., G.J.C. Schmidt, and P. Science, *Nanocomposite polymer hydrogels.* Colloid and Polymer Science, 2009. **287**(1): p. 1-11.
53. Zhang, Q., et al., *Removal of crystal violet by clay/PNIPAm nanocomposite hydrogels with various clay contents.* Applied Clay Science, 2014. **90**: p. 1-5.
54. Wang, T., et al., *Notch insensitive and self-healing PNIPAm–PAM–clay nanocomposite hydrogels.* Soft Matter, 2014. **10**(19): p. 3506-3512.

55. Wang, J., et al., *A Strong Bio-Inspired Layered PNIPAM–Clay Nanocomposite Hydrogel.* Angewandte Chemie International Edition, 2012. **51**(19): p. 4676-4680.
56. Yao, C., et al., *Poly (N-isopropylacrylamide)-clay nanocomposite hydrogels with responsive bending property as temperature-controlled manipulators.* Advanced Functional Materials., 2015. **25**(20): p. 2980-2991.
57. Chang, C.-W., et al., *PEG/clay nanocomposite hydrogel: a mechanically robust tissue engineering scaffold.* Soft Matter, 2010. **6**(20): p. 5157-5164.
58. Wang, Y., W. Wang, and A.J.C.E.J. Wang, *Efficient adsorption of methylene blue on an alginate-based nanocomposite hydrogel enhanced by organo-illite/smectite clay.* Chemical Engineering Journal. , 2013. **228**: p. 132-139.
59. Peng, N., et al., *Superabsorbent cellulose–clay nanocomposite hydrogels for highly efficient removal of dye in water.* ACS Sustainable Chemistry & Engineering, 2016. **4**(12): p. 7217-7224.
60. Xu, R., et al., *Quaternized chitosan–organic rectorite intercalated composites based nanoparticles for protein controlled release.* International journal of pharmaceutics., 2012. **438**(1-2): p. 258-265.
61. Khun, K., et al., *Potentiometric glucose sensor based on the glucose oxidase immobilized iron ferrite magnetic particle/chitosan composite modified gold coated glass electrode.* Sensors and Actuators, 2012. **173**: p. 698-703.
62. Sudheesh Kumar, P., et al., *Flexible and microporous chitosan hydrogel/nano ZnO composite bandages for wound dressing: in vitro and in vivo evaluation.* ACS applied materials & interfaces, 2012. **4**(5): p. 2618-2629.
63. Gaharwar, A.K., et al., *Highly extensible, tough, and elastomeric nanocomposite hydrogels from poly (ethylene glycol) and hydroxyapatite nanoparticles.* Biomacromolecules., 2011. **12**(5): p. 1641-1650.
64. Pina, S., J.M. Oliveira, and R.L.J.A.M. Reis, *Natural-based nanocomposites for bone tissue engineering and regenerative medicine: A review.* Advanced Materials, 2015. **27**(7): p. 1143-1169.
65. Kim, B.S., et al., *Growth and osteogenic differentiation of alveolar human bone marrow-derived mesenchymal stem cells on chitosan/hydroxyapatite composite fabric.* Journal of biomedical materials research part A., 2013. **101**(6): p. 1550-1558.
66. Servant, A., et al., *Graphene-Based Electroresponsive Scaffolds as Polymeric Implants for On-Demand Drug Delivery.* Advanced healthcare materials 2014. **3**(8): p. 1334-1343.
67. Lau, H.K. and K.L.J.B. Kiick, *Opportunities for multicomponent hybrid hydrogels in biomedical applications.* Biomacromolecules, 2014. **16**(1): p. 28-42.
68. Hancock, M.J., et al., *Anisotropic material synthesis by capillary flow in a fluid stripe.* Biomaterials., 2011. **32**(27): p. 6493-6504.
69. Blackman, M.L., M. Royzen, and J.M.J.J.o.t.A.C.S. Fox, *Tetrazine ligation: fast bioconjugation based on inverse-electron-demand Diels− Alder reactivity.* Journal of the American Chemical Society. , 2008. **130**(41): p. 13518-13519.
70. Lowe, A.B., C.E. Hoyle, and C.N.J.J.o.M.C. Bowman, *Thiol-yne click chemistry: A powerful and versatile methodology for materials synthesis.* Journal of Materials Chemistry., 2010. **20**(23): p. 4745-4750.

71. Altunbas, A., et al., *Encapsulation of curcumin in self-assembling peptide hydrogels as injectable drug delivery vehicles.* Biomaterials, 2011. **32**(25): p. 5906-5914.
72. Mulyasasmita, W., J.S. Lee, and S.C.J.B. Heilshorn, *Molecular-level engineering of protein physical hydrogels for predictive sol–gel phase behavior.* Biomacromolecules, 2011. **12**(10): p. 3406-3411.
73. Kolambkar, Y.M., et al., *An alginate-based hybrid system for growth factor delivery in the functional repair of large bone defects.* Biomaterials, 2011. **32**(1): p. 65-74.
74. Chen, J., et al., *Reducible polyamidoamine-magnetic iron oxide self-assembled nanoparticles for doxorubicin delivery.* Biomaterials, 2014. **35**(4): p. 1240-1248.
75. Zhang, Y.N., et al., *A highly elastic and rapidly crosslinkable elastin-like polypeptide-based hydrogel for biomedical applications.* Advanced Functional Materials, 2015. **25**(30): p. 4814-4826.
76. Kim, Y., J.N. Renner, and J.C.J.B.S. Liu, *Incorporating the BMP-2 peptide in genetically-engineered biomaterials accelerates osteogenic differentiation.* Biomaterials Science, 2014. **2**(8): p. 1110-1119.
77. Cui, F., et al., *Hyaluronic acid hydrogel immobilized with RGD peptides for brain tissue engineering.* Journal of Materials Science: Materials in Medicine., 2006. **17**(12): p. 1393-1401.
78. Chau, Y., et al., *Incorporation of a matrix metalloproteinase-sensitive substrate into self-assembling peptides–a model for biofunctional scaffolds.* Biomaterials, 2008. **29**(11): p. 1713-1719.
79. Qu, Y., et al., *A biodegradable thermo-responsive hybrid hydrogel: therapeutic applications in preventing the post-operative recurrence of breast cancer.* NPG Asia Materials, 2015. **7**(8): p. e207.
80. Kim, Y.-M., M.-R. Park, and S.-C.J.A.n. Song, *Injectable polyplex hydrogel for localized and long-term delivery of siRNA.* acs nano, 2012. **6**(7): p. 5757-5766.
81. Sun, T.L., et al., *Physical hydrogels composed of polyampholytes demonstrate high toughness and viscoelasticity.* Nature Materials, 2013. **12**(10): p. 932.
82. Sun, J.-Y., et al., *Highly stretchable and tough hydrogels.* nature, 2012. **489**(7414): p. 133.
83. Sun, J.-Y., et al., *Highly stretchable and tough hydrogels.* Nature Materials, 2012. **489**(7414): p. 133.
84. Li, J., Z. Suo, and J.J.J.J.o.M.C.B. Vlassak, *Stiff, strong, and tough hydrogels with good chemical stability.* Journal of Materials Chemistry B. , 2014. **2**(39): p. 6708-6713.
85. Lo, C.-M., et al., *Cell movement is guided by the rigidity of the substrate.* Biophysical journal. , 2000. **79**(1): p. 144-152.
86. Mitrossilis, D., et al., *Real-time single-cell response to stiffness.* Proc Natl Acad Sci U S A, 2010. **107**(38): p. 16518-23.
87. Hadjipanayi, E., V. Mudera, and R.A. Brown, *Guiding cell migration in 3D: a collagen matrix with graded directional stiffness.* Cell Motil Cytoskeleton, 2009. **66**(3): p. 121-8.
88. Trotter, J.A., et al., *Collagen fibril aggregation-inhibitor from sea cucumber dermis.* Matrix Biology, 1999. **18**(6): p. 569-578.
89. Trotter, J.A., et al., *Stiparin: a glycoprotein from sea cucumber dermis that aggregates collagen fibrils.* Matrix Biol, 1996. **15**(2): p. 99-110.
90. Capadona, J.R., et al., *Stimuli-responsive polymer nanocomposites inspired by the sea*

cucumber dermis. science, 2008. **319**(5868): p. 1370-1374.
91. Shanmuganathan, K., et al., *Bio-inspired mechanically-adaptive nanocomposites derived from cotton cellulose whiskers.* Journal of Materials Chemistry. , 2010. **20**(1): p. 180-186.
92. Dagnon, K.L., et al., *Water-triggered modulus changes of cellulose nanofiber nanocomposites with hydrophobic polymer matrices.* macromolecules, 2012. **45**(11): p. 4707-4715.
93. Shanmuganathan, K., et al., *Stimuli-responsive mechanically adaptive polymer nanocomposites.* ACS applied materials & interfaces., 2009. **2**(1): p. 165-174.
94. Liu, M., et al., *The improvement of mechanical performance and water-response of carboxylated SBR by chitin nanocrystals.* European Polymer Journal. , 2015. **68**: p. 190-206.
95. Way, A.E., et al., *pH-responsive cellulose nanocrystal gels and nanocomposites.* ACS Macro Letters, 2012. **1**(8): p. 1001-1006.
96. Yang, W.J., et al., *Antifouling and antibacterial hydrogel coatings with self-healing properties based on a dynamic disulfide exchange reaction.* Polymer Chemistry., 2015. **6**(39): p. 7027-7035.
97. Yang, B., et al., *Facilely prepared inexpensive and biocompatible self-healing hydrogel: a new injectable cell therapy carrier.* Polymer Chemistry. , 2012. **3**(12): p. 3235-3238.
98. Tseng, T.C., et al., *An injectable, self-healing hydrogel to repair the central nervous system.* Advanced Materials, 2015. **27**(23): p. 3518-3524.
99. Cai, L., R.E. Dewi, and S.C.J.A.f.m. Heilshorn, *Injectable hydrogels with in situ double network formation enhance retention of transplanted stem cells.* Advanced functional materials. , 2015. **25**(9): p. 1344-1351.
100. Algi, M.P. and O.J.E.P.J. Okay, *Highly stretchable self-healing poly (N, N-dimethylacrylamide) hydrogels.* European Polymer Journal, 2014. **59**: p. 113-121.
101. Deng, G., et al., *Dynamic hydrogels with an environmental adaptive self-healing ability and dual responsive sol–gel transitions.* ACS Macro Letters, 2012. **1**(2): p. 275-279.
102. Liu, B., et al., *Hydrogen bonds autonomously powered gelatin methacrylate hydrogels with super-elasticity, self-heal and underwater self-adhesion for sutureless skin and stomach surgery and E-skin.* biomaterials, 2018. **171**: p. 83-96.
103. Darabi, M.A., et al., *Skin-Inspired Multifunctional Autonomic-Intrinsic Conductive Self-Healing Hydrogels with Pressure Sensitivity, Stretchability, and 3D Printability.* advanced materials, 2017. **29**(31): p. 1700533.
104. Jiang, G., et al., *Network structure and compositional effects on tensile mechanical properties of hydrophobic association hydrogels with high mechanical strength.* Polymer. , 2010. **51**(6): p. 1507-1515.
105. Lee, J.Y., G.A. Buxton, and A.C.J.T.J.o.c.p. Balazs, *Using nanoparticles to create self-healing composites.* The Journal of chemical physics. , 2004. **121**(11): p. 5531-5540.
106. Gupta, S., et al., *Entropy-driven segregation of nanoparticles to cracks in multilayered composite polymer structures.* Nature Materials. , 2006. **5**(3): p. 229.
107. White, S.R., et al., *Autonomic healing of polymer composites.* nature, 2001. **409**(6822): p. 794.
108. He, L., et al., *pH responsive self-healing hydrogels formed by boronate–catechol*

complexation. Chemical Communications. , 2011. **47**(26): p. 7497-7499.
109. Nakahata, M., et al., *Redox-responsive self-healing materials formed from host–guest polymers.* Nature communications, 2011. **2**: p. 511.
110. Lee, B.P. and S.J.A.M. Konst, *Novel hydrogel actuator inspired by reversible mussel adhesive protein chemistry.* 2014. **26**(21): p. 3415-3419.
111. Li, X. and M.J.J.A.F.M. Serpe, *Understanding the Shape Memory Behavior of Self - Bending Materials and Their Use as Sensors.* 2016. **26**(19): p. 3282-3290.
112. Lendlein, A. and R.J.S. Langer, *Biodegradable, elastic shape-memory polymers for potential biomedical applications.* science, 2002. **296**(5573): p. 1673-1676.
113. Maitland, D.J., et al., *Photothermal properties of shape memory polymer micro -actuators for treating stroke.* Lasers in Surgery and Medicine: The Official Journal of the American Society for Laser Medicine and Surgery, 2002. **30**(1): p. 1-11.
114. Schmidt, A.M.J.M.R.C., *Electromagnetic activation of shape memory polymer networks containing magnetic nanoparticles.* Macromolecular Rapid Communications., 2006. **27**(14): p. 1168-1172.
115. Liu, C., H. Qin, and P.J.J.o.m.c. Mather, *Review of progress in shape-memory polymers.* Journal of materials chemistry., 2007. **17**(16): p. 1543-1558.
116. Wache, H., et al., *Development of a polymer stent with shape memory effect as a drug delivery system.* Journal of Materials Science: Materials in Medicine., 2003. **14**(2): p. 109-112.
117. Gall, K., et al., *Thermomechanics of the shape memory effect in polymers for biomedical applications.* Journal of Biomedical Materials Research Part A: An Official Journal of The Society for Biomaterials, The Japanese Society for Biomaterials, and The Australian Society for Biomaterials and the Korean Society for Biomaterials., 2005. **73**(3): p. 339-348.
118. Tanaka, Y., et al., *Thermoreversible transition of tensile modulus of hydrogel with ordered aggregates.* Macromolecules., 1995. **28**(7): p. 2574-2576.
119. Osada, Y. and A.J.N. Matsuda, *Shape memory in hydrogels.* nature, 1995. **376**(6537): p. 219.
120. Hao, J. and R.J.A.M.L. Weiss, *Mechanically tough, thermally activated shape memory hydrogels.* ACS Macro Letters, 2013. **2**(1): p. 86-89.
121. Leng, J., et al., *Shape-memory polymers and their composites: stimulus methods and applications.* Progress in Materials Science, 2011. **56**(7): p. 1077-1135.
122. Mendez, J., et al., *Bioinspired mechanically adaptive polymer nanocomposites with water-activated shape-memory effect.* 2011. **44**(17): p. 6827-6835.
123. Guo, W., et al., *Switchable Bifunctional Stimuli - Triggered Poly - N - Isopropylacrylamide/DNA Hydrogels.* Angewandte Chemie International Edition., 2014. **53**(38): p. 10134-10138.
124. Augst, A.D., H.J. Kong, and D.J.J.M.b. Mooney, *Alginate hydrogels as biomaterials.* Macromolecular bioscience., 2006. **6**(8): p. 623-633.
125. Jayakumar, R., et al., *Biomaterials based on chitin and chitosan in wound dressing applications.* Biotechnology advances, 2011. **29**(3): p. 322-337.
126. Nichol, J.W., et al., *Cell-laden microengineered gelatin methacrylate hydrogels.*

Biomaterials, 2010. **31**(21): p. 5536-5544.
127. Chang, C. and L.J.C.p. Zhang, *Cellulose-based hydrogels: present status and application prospects.* Carbohydrate polymers, 2011. **84**(1): p. 40-53.
128. Luo, Y., K.R. Kirker, and G.D.J.J.o.c.r. Prestwich, *Cross-linked hyaluronic acid hydrogel films: new biomaterials for drug delivery.* Journal of controlled release, 2000. **69**(1): p. 169-184.
129. Burdick, J.A. and G.D.J.A.m. Prestwich, *Hyaluronic acid hydrogels for biomedical applications.* Advanced materials, 2011. **23**(12): p. H41-H56.
130. Kumar, M.N.R.J.R. and f. polymers, *A review of chitin and chitosan applications.* 2000. **46**(1): p. 1-27.
131. Torrado, S.J.B., *Interpolymer complexes of poly (acrylic acid) and chitosan: influence of the ionic hydrogel-forming medium.* Biomaterials, 2003. **24**(8): p. 1459-1468.
132. Lin, Y.-H., et al., *Physically crosslinked alginate/N, O-carboxymethyl chitosan hydrogels with calcium for oral delivery of protein drugs.* biomaterials, 2005. **26**(14): p. 2105-2113.
133. Di Martino, A., M. Sittinger, and M.V.J.B. Risbud, *Chitosan: a versatile biopolymer for orthopaedic tissue-engineering.* Biomaterials, 2005. **26**(30): p. 5983-5990.
134. Shu, X., K. Zhu, and W.J.I.j.o.p. Song, *Novel pH-sensitive citrate cross-linked chitosan film for drug controlled release.* International journal of pharmaceutics, 2001. **212**(1): p. 19-28.
135. Bidgoli, H., A. Zamani, and M.J.J.C.r. Taherzadeh, *Effect of carboxymethylation conditions on the water-binding capacity of chitosan-based superabsorbents.* Carbohydrate research, 2010. **345**(18): p. 2683-2689.
136. An, N.T., N.T. Dong, and P.J.C.P. Le Dung, *Water-soluble N-carboxymethylchitosan derivatives: Preparation, characteristics and its application.* Carbohydrate Polymers. , 2009. **75**(3): p. 489-497.
137. Hon, D.N.S. and L.G.J.J.o.A.P.S. Tang, *Chelation of chitosan derivatives with zinc ions. I. O, N-carboxymethyl chitosan.* journal of Applied Polymer Science, 2000. **77**(10): p. 2246-2253.
138. Chen, L., Z. Tian, and Y.J.B. Du, *Synthesis and pH sensitivity of carboxymethyl chitosan-based polyampholyte hydrogels for protein carrier matrices.* Biomaterials. , 2004. **25**(17): p. 3725-3732.
139. Muzzarelli, R.A., et al., *N-(carboxymethylidene) chitosans and N-(carboxymethyl) chitosans: Novel chelating polyampholytes obtained from chitosan glyoxylate.* Carbohydrate Research., 1982. **107**(2): p. 199-214.
140. Thanou, M., et al., *Mono-N-carboxymethyl chitosan (MCC), a polyampholytic chitosan derivative, enhances the intestinal absorption of low molecular weight heparin across intestinal epithelia in vitro and in vivo.* Journal of pharmaceutical sciences, 2001. **90**(1): p. 38-46.
141. Song, Q., et al., *Synthesis and property studies of N-carboxymethyl chitosan.* Journal of Applied Polymer Science, 2011. **119**(6): p. 3282-3285.
142. Muzzarelli, R.A., P. Ilari, and M.J.I.j.o.b.m. Petrarulo, *Solubility and structure of N-carboxymethylchitosan.* International journal of biological macromolecules. , 1994. **16**(4): p. 177-180.

143. Chen, S.-C., et al., *A novel pH-sensitive hydrogel composed of N, O-carboxymethyl chitosan and alginate cross-linked by genipin for protein drug delivery.* Journal of Controlled Release, 2004. **96**(2): p. 285-300.
144. Guo, Z., et al., *Synthesis and hydroxyl radicals scavenging activity of quaternized carboxymethyl chitosan.* Carbohydrate Polymers, 2008. **73**(1): p. 173-177.
145. Weng, L., X. Chen, and W.J.B. Chen, *Rheological characterization of in situ crosslinkable hydrogels formulated from oxidized dextran and N-carboxyethyl chitosan.* Biomacromolecules, 2007. **8**(4): p. 1109-1115.
146. Ghosh, K., et al., *Rheological characterization of in situ cross-linkable hyaluronan hydrogels.* Biomacromolecules, 2005. **6**(5): p. 2857-2865.
147. Liu, B., et al., *Hydrogen bonds autonomously powered gelatin methacrylate hydrogels with super-elasticity, self-heal and underwater self-adhesion for sutureless skin and stomach surgery and E-skin.* Biomaterials, 2018. **171**: p. 83-96.
148. Yui, T., et al., *Molecular and crystal structure of the anhydrous form of chitosan.* Macromolecules, 1994. **27**(26): p. 7601-7605.
149. Darabi, M.A., et al., *Gum Sensor: A Stretchable, Wearable, and Foldable Sensor Based on Carbon Nanotube/Chewing Gum Membrane.* ACS Appl Mater Interfaces, 2015. **7**(47): p. 26195-205.
150. Darabi, M.A., et al., *Skin-inspired multifunctional autonomic-intrinsic conductive self-healing hydrogels with pressure sensitivity, stretchability, and 3D printability.* 2017. **29**(31): p. 1700533.
151. Deng, Z., et al., *Multifunctional stimuli-responsive hydrogels with self-healing, high conductivity, and rapid recovery through host–guest interactions.* 2018. **30**(5): p. 1729-1742.
152. Hong, S.M., et al., *3D Printing of Highly Stretchable and Tough Hydrogels into Complex, Cellularized Structures.* Advanced Materials, 2015. **27**(27): p. 4035-4040.
153. Rutz, A.L., et al., *A Multimaterial Bioink Method for 3D Printing Tunable, Cell-Compatible Hydrogels.* Advanced Materials, 2015. **27**(9): p. 1607-+.

Appendix

西安立飞生物科技有限公司
Xi'an Lyphar Biotech Co., Ltd

Certificate of Analysis

Product Name:	Carboxymethyl Chitosan	Manufacture Date:	Mar.05, 2016
Batch Number:	Lyph20160505	Certificate Date:	Mar.05, 2016
Batch Quantity:	559 Kg	Expiration Date	Mar.05, 2018

ITEM	STANDARD	TESTING RESULT
Appearance	Off-White Powder	Comply
Degree of Substitution %	≥80%	82%
Viscosity(1%@25℃)	≤100mpa.s	20mpa.s
Moisture	≤15.00%	12.8%
Ash	≤1.0%	0.86%
DAC Degree	≥95.00%	96.1%
PH	7.0～8.0	7.6
Arsenic	≤0.5ppm	＜0.5ppm
Heavy metais	≤20ppm	＜10ppm
Particle Size	95%Through 60 Mesh Sieve	Comply
Total Plate Count	≤3000cfu/g	＜1000cfu/g
Molds &Yeast	≤100cfu/g	＜100cfu/g
E.Coli	Negative	Negative
Salmonella	Negative	Negative

Conclusion	Conform with specification
Storage	Store in cool & dry place not freeze, keep away from strong light and heat
Shelf life	2 years when properly stored

Quality Assurance Officer:董文华　　**Corrector:** 王君　　**Analyst:**李丽

Xi'an Lyphar Biotech Co., LTD Tel.: 0086-29-89196322 Fax: 0086-29-88891941
Add:No. 11, The South of Tangyan Road, Hi-Tech Industrial Zone, Xi'an City, Shaanxi Province, China
Email: sales@lyphar.com Web: www.lyphar.com

Figure 24 Product information sheet of CM.